Table 2 Genotyping results for genes in the human Chr 1 region homologous to the mouse *Ath1* locus

Gene[a]	RefSNP ID[b]	SNP[c]	Position in gene (bp in Ensembl)	Rare alleles, % (total alleles) Affected	Control	*P*
PIGC	rs1063412	C/T	Exon 2 coding (169650343)	40.7 (684)	41.7 (734)	0.69
C1orf9[d]	rs1053381	A/G	3′ UTR (169819913)	6.3 (694)	8.0 (672)	0.22
TNFSF6 (FASL)	rs763110	C/T	687 bp upstream (169866874)	31.6 (728)	32.0 (744)	0.87
Intergenic	rs983514	A/T	(170111828)	3.0 (708)	3.5 (714)	0.57
TNFSF18	rs1883477	A/G	Intron 1 (170258429)	19.0 (694)	18.3 (706)	0.72
TNFSF4 (OX40L)	rs1234315	C/T	1,992 bp upstream (170417839)[f]	45.9 (754)	43.3 (778)	0.31
	rs3850641	A/G	Intron 1 (170415208)[e]	15.5 (766)	12.1 (784)	0.05
	rs1234313	A/G	Intron 1 (170405623)[e]	29.6 (766)	33.4 (784)	0.11
	rs3861950	C/T	Intron 2 (170395668)[e]	33.4 (710)	30.4 (746)	0.23
	rs1234312	C/T	1,809 bp downstream (170390438)[f]	3.0 (766)	2.6 (772)	0.62
PRDX6	rs7314	C/T	3′ UTR (170696975)	26.6 (732)	25.8 (730)	0.70
KHLX[d]	rs2273366	A/G	Intron 3 (170964318)	26.6 (696)	28.5 (738)	0.22
Intergenic	rs2235095	C/T	(171073981)	10.0 (730)	10.9 (714)	0.57
SERPINC1 (AT3)	rs5878	A/G	Exon 5 coding (171118208)	31.6 (712)	34.1 (704)	0.32
Q8IVE6[d]	rs1884994	C/T	Exon 4 (171189658)	18.1 (684)	18.1 (684)	NS

[a]Genes and intergenic segments in the table are listed from proximal to distal Chr 1. *PIGC*, phosphatidylinositol-glycan biosynthesis; *C1orf9*, class C protein, chromosome 1 open reading frame 9; *TNFSF6*, tumor necrosis factor ligand superfamily member 6 (Fas ligand); *TNFSF18*, tumor necrosis factor ligand superfamily member 18; *TNFSF4*, tumor necrosis factor ligand superfamily member 4 (OX40 ligand); *PRDX6*, peroxiredoxin 6; *KHLX*, Kelch-like protein X; *SERPINC1*, serine (or cysteine) proteinase inhibitor, clade C, member 1. [b]National Center for Biotechnology Information SNP database build 116. [c]Ancestral allele/rare allele. [d]Putative gene. [e]In reverse order in Ensembl Human Genome Browser.

and had lower plasma concentrations of both HDL cholesterol and LDL cholesterol than did controls. We initially tested one SNP (rs3850641) in *TNFSF4* and found that a rare allele (G) was significantly more common ($P = 0.05$) in affected individuals than in controls (**Table 2**). We then tested four additional SNPs in *TNFSF4*, which, together with the one already tested (rs3850641), were evenly distributed across the *TNFSF4* gene. The allele frequencies of these four additional *TNFSF4* SNPs were not significantly different in affected individuals versus the controls. The significance of the allele frequency differences gradually decreased on either side of rs3850641, further suggesting that the difference in its allele frequency in affected individuals versus controls was real. Finally, we tested one SNP from each of eight genes around *TNFSF4* (**Fig. 1b**), under the hypothesis that none of them would underlie *Ath1* or be significantly different. Consistent with this hypothesis, none of these SNPs differed in affected individuals versus controls (**Table 2**). The genotype distributions of all the SNPs we tested were in Hardy-Weinberg equilibrium (data not shown). By using the EMLD program to calculate the pairwise linkage disequilibrium coefficients for the five *TNFSF4* SNPs, we found a high degree of linkage disequilibrium between rs1234315, rs3850641 and rs1234313, and between rs1234313, rs3861950 and rs1234312 (**Supplementary Table 2** online).

We then tested the association of the SNP rs3850641 with myocardial infarction in a second human population from the Stockholm Heart Epidemiology Program (SHEEP). The percentage of total alleles that were rare alleles was greater in females with myocardial infarction than in female controls (16.9% of 674 versus 13.4% of 964; $P = 0.05$) but was not significantly different in males with myocardial infarction versus male controls or in all individuals with myocardial infarction versus all controls (data not shown). In both populations, the genotype of the SNP rs3850641 was associated with an increased risk of myocardial infarction in women but not in men (**Table 3**), indicating that this haplotype has a gender-specific effect.

TNFSF4 haplotypes associated with coronary artery disease

Of 32 haplotypes possible from the five *TNFSF4* SNPs, eight were present in 97.5% of the subjects (affected individuals and controls combined; **Table 4**). Haplotypes 11000, 11010 and 110NN (the first two combined) were significantly ($P = 0.03$, 0.03 and 0.01, respectively) more frequent in individuals with coronary artery disease (diagnosed with coronary angiography) than in controls. In contrast, haplotype 00100 (with first three SNPs all different from the corresponding ones in haplotype 110NN) was significantly more frequent ($P = 0.02$) in controls than in affected individuals. This result suggests that the first three SNPs, which are in linkage disequilibrium with each other, determine the distribution frequency of *TNFSF4* haplotypes.

TNFSF4 haplotypes were associated not only with risk of coronary artery disease but also with degree of stenosis and some risk factors in this disease. Affected individuals with the 110NN haplotype had less severe coronary artery stenosis than did those with other haplotypes (30.1% versus 32.7% stenosis; $P = 0.05$). Controls carrying the 110NN

Table 3 Relative risk of myocardial infarction estimated by odds ratio in carriers of the G allele of rs3850641

	SCARF			SHEEP		
	Women	Men	Women and men	Women	Men	Women and men
Crude[a]	2.8 (1.3–6.3)	1.2 (0.8–1.7)	1.4 (1.0–1.9)	1.3 (1.0–1.8)	1.0 (0.8–1.2)	1.1 (0.9–1.3)
Adjusted[b]	5.9 (1.6–22.0)	1.1 (0.7–1.7)	1.4 (0.9–2.0)	1.3 (1.0–1.8)	0.9 (0.7–1.1)	1.0 (0.9–1.2)

[a]Adjusted for age and residential area. [b]Adjusted for age, HDL, LDL, triglyceride, BMI, smoking and residential area.

Table 4 Distribution of the most frequently occurring *TNFSF4* haplotypes in individuals with coronary artery disease and controls

Haplotype	Total (%)	Control (%)	Affected (%)	*P*
00000	117 (7.5)	55 (47.0)	62 (53.0)	0.60
00001	30 (1.9)	15 (50.0)	15 (50.0)	1.00
00100	453 (29.2)	244 (53.9)	209 (46.1)	0.02
11000	47 (3.0)	21 (44.7)	26 (55.3)	0.03
11010	162 (10.5)	71 (43.8)	91 (56.2)	0.03
11ONN	210 (13.5)	92 (43.8)	118 (56.2)	0.01
10010	78 (5.0)	44 (56.4)	34 (43.6)	0.61
00010	243 (15.7)	125 (51.4)	118 (48.6)	0.52
10000	382 (24.6)	194 (50.8)	188 (49.2)	0.66
Sum*	1,512 (97.5)			

A total of 775 controls (1,550 alleles) are included in the table. *P* values were calculated using the χ^2 test for genotype distribution. N, any possible genotype; 0, ancestral allele; 1, rare allele.
*11ONN haplotype not included in total.

haplotype had significantly higher plasma HDL cholesterol ($P = 0.02$) and serum amyloid A ($P = 0.007$) levels than those carrying other haplotypes (**Supplementary Table 3** online).

DISCUSSION

QTL mapping has been used to identify genetic loci that control complex traits, including atherosclerosis. Thus far, 20 mouse and 18 human QTLs for atherosclerosis have been reported (X.W. and B.P., unpublished data), but the gene (5-lipoxygenase) underlying only one of these QTLs (*Artles*) has been identified[12]. Here we report evidence that *Tnfsf4* underlies *Ath1* and that polymorphisms in *TNFSF4* may contribute to the development of myocardial infarction and coronary artery disease in humans.

We arrived at these conclusions by testing the best candidates for underlying *Ath1* in the mouse: *Prdx6*, *Tnfsf6* and *Tnfsf4*. Although PRDX6 is an effective antioxidant, protects mice against oxidative stress[5] and could therefore potentially inhibit atherogenesis, we previously found evidence that *Prdx6* is unlikely to underlie *Ath1* (refs. 6,7). Here we report the results of testing the other two candidates: *Tnfsf6* and *Tnfsf4*. The hallmark of early atherosclerosis is the formation of foam cells derived from macrophages and smooth muscle cells after they have taken up cholesterol esters. Lymphocytes are important in atherogenesis[10]. T, B and NK cells have all been identified in atherosclerotic lesions[10]. It is generally believed that T lymphocytes[13] and NK cells[14] are proatherogenic, and B lymphocytes are antiatherogenic[15,16]. Depleting mice of both T and B lymphocytes inhibits atherosclerosis[17], at least at early stages[18,19]. We chose *Tnfsf6* and *Tnfsf4* as candidates for underlying *Ath1* for two reasons. First, they are both expressed on endothelial cells, lymphocytes and macrophages. Second, they both control the proliferation and survival of lymphocytes[8,9], though in seemingly antagonistic ways: whereas the FASL-FAS pathway leads to lymphocyte apoptosis[8,20], the OX40L-OX40 pathway leads to lymphocyte proliferation and survival[9].

We tested the possibility that *Tnfsf6* underlies *Ath1* in C3H *Tnfsf6*^{gld} mice, which are naturally deficient in *Tnfsf6*. Overexpressed FASL on endothelial cells decreases atherosclerosis and infiltration of macrophages and CD8 T cells into the lesions in *Apoe*-deficient mice[21]. *Tnfsf6* mutation had an opposite effect[22], suggesting that FASL is antiatherosclerotic. We therefore rationalized that if *Tnfsf6* underlay *Ath1* and its C3H allele makes C3H mice resistant to atherosclerosis, then C3H mice with nonfunctional *Tnfsf6* should lose their resistance and become susceptible to atherosclerosis. We found, however, that C3H *Tnfsf6*^{gld} mice were as resistant to atherosclerosis as were controls, suggesting that *Tnfsf6* did not underlie *Ath1*. Even though *Tnfsf6* probably does not underlie *Ath1*, however, it may affect atherogenesis, possibly depending on the stage of atherosclerosis[20] and the particular animal model used (FASL was proatherosclerotic in rabbits[23] and antiatherosclerotic in mice[21,22]).

The third candidate we tested was *Tnfsf4*. We conclude that *Tnfsf4* underlies *Ath1* on the basis of the following observations. First, OX40L is proatherogenic in mice. *Tnfsf4*$^{-/-}$ mice on an atherosclerosis-susceptible B6 background were more resistant to atherosclerosis than were B6 mice. Although these knockouts had 129 alleles between 153.3 Mb and 162.7 Mb on Chr 1, they did not confer resistance to atherosclerosis because *Prdx6*$^{-/-}$ mice with 129 alleles in the same region were as susceptible to atherosclerosis as were B6 controls[7]. Therefore, *Tnfsf4*$^{-/-}$ mice must have been more resistant to atherosclerosis than were controls because their *Tnfsf4* gene was knocked out. The proatherogenic role of OX40L was further verified by using B6 mice overexpressing *Tnfsf4*, which had significantly larger atherosclerotic lesions than did the controls.

Second, the higher mRNA expression of *Tnfsf4* in B6 aortas than in comparable C3H aortas is consistent with the idea that *Tnfsf4* is proatherogenic. In mice, polymorphisms exist between B6 and C3H strains in the potential regulatory regions of *Tnfsf4*. In humans, a SNP in the first intron of *TNFSF4* and haplotypes consisting of a SNP upstream of exon 1 and two SNPs in the first intron of *TNFSF4* (all in the potential regulatory regions) were associated with risk of myocardial infarction and coronary artery disease, respectively, again suggesting that polymorphisms in the potential regulatory regions of *TNFSF4* affected its functional levels. The fact that we could replicate the significant association in two independent populations, in females but not in males in both cases, suggests that the association is real.

Third, the functions of OX40L can be linked to the development of atherosclerosis. Activation of the OX40L-OX40 pathway enhances the proliferation and survival of T cells, which are proatherogenic. In addition, OX40L was expressed in endothelial cells, macrophages, smooth muscles and lymphocytes in mouse atherosclerotic lesions, suggesting that OX40L participates in atherogenesis. Furthermore, incubation of human umbilical vein endothelial cells with recombinant OX40 induces RANTES-CCL5 (ref. 24), a member of C-C chemokines that functions as a chemoattractant for proatherogenic monocytes and T cells[25].

Fourth, a mouse atherosclerosis QTL (*Athsq1*) was found on Chr 4 at 77 cM (ref. 26), near where *Tnfrsf4* (also called *Ox40*, which encodes the receptor of OX40L) is located (79 cM). Because *Athsq1* was found in (MOLF/Ei × B6.129S7 *Ldlr*^{tm1Her}) × C57BL/6J *Ldlr*^{tm1Her} backcross mice, we sequenced *Tnfrsf4* in both parental strains and found that MOFL OX40 had a 15–amino acid insertion (TVQSTTVQSTTVQST) between amino acids 190 and 191 and a H277Q substitution (X.W. and B.P., unpublished data). This finding, combined with our results indicating that *Tnfsf4* underlies *Ath1*, suggests that the OX40L-OX40 pathway participates in atherogenesis in mice.

Fifth, a human linkage study identified a QTL (lod = 2.4, genome-wide $P < 0.05$) for early-onset coronary artery disease on chromosome 1q25 (ref. 27). This human QTL is homologous to mouse *Ath1* and *TNFSF4* lies right under the peak of the lod score curve. Our study suggests that *TNFSF4* is an excellent candidate to underlie this QTL.

Sixth, a QTL for human myocardial infarction was recently mapped to 1p34–36 (ref. 28). Its mouse homologous region is between 58 cM and 83 cM on Chr 4, where *Athsq1* (77 cM) is located. The gene encoding OX40 underlies the QTL in both species, further suggesting that the OX40L-OX40 pathway participates in atherosclerosis in both species.

Although there is no 'gold standard' for positively identifying a gene underlying a QTL, the Complex Trait Consortium suggested that a candidate gene should meet more than one of these eight criteria[29]: (i) polymorphisms in either coding or regulatory regions have been found; (ii) its function has been linked to the quantitative trait being analyzed; (iii) its function has been tested *in vitro*; (iv) its function has been tested in transgenic animals; (v) its function has been tested in knock-in animals; (vi) its function has been assessed in deficiency-complementation test; (vii) its function has been tested by mutational analysis; and (viii) a homologous QTL for the same phenotype in another species has been found. *Tnfsf4* meets six of these criteria (i–iv, vii and viii), and an additional criterion that we propose: its receptor underlies the QTL for the same phenotype. Therefore, we conclude, on the basis of positionally cloning, that *Tnfsf4* underlies *Ath1* and that *TNFSF4* may also participate in human atherosclerosis.

One remaining question is whether the gene underlying *Ath1* controls both atherosclerosis susceptibility and HDL cholesterol levels. Both *Prdx6*$^{-/-}$ (ref. 7) and *Tnfsf4*$^{-/-}$ mice had higher plasma HDL cholesterol levels than did controls. We think it unlikely that mutations in both *Prdx6* and *Tnfsf4* led to the increased plasma HDL cholesterol levels. Rather, the 129 allele(s) of other gene(s) in the congenic region (both knockouts are congenics on B6 background with 129 alleles in *Ath1* region) may cause elevated HDL cholesterol levels. Despite increased plasma HDL cholesterol levels in both *Prdx6*$^{-/-}$ and *Tnfsf4*$^{-/-}$ mice, only the latter had decreased atherosclerotic lesions, suggesting that *Tnfsf4* promotes atherogenesis independent of plasma HDL cholesterol levels.

The results of our study are important for three primary reasons. First, we proved that positional cloning of a gene underlying a mouse QTL could lead to identifying the homologous gene contributing to human disease. After identifying the gene in the mouse, we were able to test it in human populations in a hypothesis-driven association study, which is more powerful statistically than the typical association study that tests multiple genes with no *a priori* hypothesis. For example, because animal studies provided the hypothesis that *Tnfsf4* underlies *Ath1*, we could test the human population accepting a *P* value for significance of 0.05. Had we tested each of the nine genes in the *Ath1* region with no prior hypothesis, we would have had to correct the *P* value for multiple testing; making a conservative Bonferroni correction and dividing the *P* value of 0.05 by the nine independent tests would have resulted in the requirement of a *P* value of 0.0055 for significance. Thus, using the animal model to generate a hypothesis results in more efficient study of human populations.

Second, these data will encourage further studies of the OX40L-OX40 pathway in atherosclerosis. Myocardial infarction is often caused by plaque rupture of the lesions with thin fibrous caps, rather than at the most stenotic sites[30]. Factors promoting lesion growth and smooth muscle proliferation tend to make the cap thicker and stabilize the lesions, and factors inhibiting the growth of fibrous lesions may destabilize the lesions and trigger plaque rupture. In fact, unstable plaques are particularly rich in activated lymphocytes, suggesting that they may participate in plaque rupture[10]. 110NN carriers might have an increased risk of early myocardial infarction because they are prone to plaque rapture secondary to an inflammatory state associated with genetic variation in *TNFSF4*, despite having higher HDL levels and less severe stenosis. Future studies need to address these possibilities. It is not known why the 110NN haplotype was associated with an increased risk of myocardial infarction in women but not in men. We previously found a gender-dependent association of polymorphisms of toll-like receptor 4, essential for innate immunity, with the risk of myocardial infarction[31], suggesting that gender-related factors affect immune reactions in atherosclerosis. This gender-specific effect was also found in mice: female B6 mice are more susceptible to atherosclerosis than are male B6 mice[32].

Third, the OX40L-OX40 pathway may be an excellent target for atherosclerosis therapy. The expression of OX40L in all the major cell types in atherosclerotic lesions (endothelial cells, lymphocytes, macrophages and smooth muscle cells) suggests that it has a central role in regulating and coordinating inflammatory mediators from various types of cells in atherosclerotic lesions. Additionally, both OX40L and OX40 are expressed more highly in inflammatory than in normal tissues[9]. Therefore, targeting the OX40L-OX40 pathway may inhibit local inflammation and the function of OX40L on nonimmune cells without jeopardizing global immune competence. Furthermore, the OX40L-OX40 interaction has been targeted for treating many chronic inflammatory diseases[33], such as graft-versus-host disease, experimental allergic encephalomyelitis, inflammatory bowel diseases, rheumatoid arthritis, asthma, tumor formation, diabetes and HIV-1 infection. Atherosclerosis may be the next disease to be targeted.

METHODS

Mice and diet. We obtained B6, C3H and C3H/HeJ *Tnfsf6*^{gld} mice from the Jackson Laboratory. Mice with targeted mutation of *Tnfsf4* (*Tnfsf4*$^{-/-}$) were on a B6 background[34]: all the alleles between *D1Mit346* (151.3 Mb) and *D1Mit504* (162.7 Mb; *Tnfsf4* is at 162.0 Mb) on Chr 1 were homozygous with respect to 129, and the rest of the genome was homozygous with respect to B6. We maintained *Tnfsf4*$^{-/-}$ mice by intercrossing and used littermate wild-type mice as controls. We generated B6 mice carrying the transgene of B6 *Tnfsf4* cDNA under the control of the ubiquitous metallothionein (Mt) promoter as described[6]. We amplified the cDNA from mouse spleens using specific primers (**Supplementary Table 4** online) and then inserted the 0.87-kb fragment into the pCR2.1 TOPO TA vector. We linked the end of the 3′ cDNA (without poly-A signal) to a fragment of the human growth hormone gene. The latter fragment was introduced to allow us to distinguish transgenic from endogenous cDNA expression. The final construct also carries an intron (beta globin IVS intron) between promoter and cDNA to enhance expression. We genotyped the *Tnfsf4* transgene by PCR (primers sequences are shown in **Supplementary Table 4** online). We obtained a 670-bp product from transgenic mice. *Tnfsf4* transgenic mice expressed much higher levels of *Tnfsf4* mRNA than did the littermate nontransgenic controls (*Tnfsf4* mRNA copies per 1,000 copies of β-actin mRNA in liver: 570 ± 149 and 2 ± 1; in aorta: 579 ± 113 and 18 ± 7; in heart: 190 ± 29 and 26 ± 4; and in spleen: 67 ± 13 and 15 ± 4 for transgenics and controls, respectively; mean ± s.e.m., $n = 3$ in each group; $P < 0.01$ for all comparisons). We retrieved the genetic positions of all the markers and genes from Mouse Genome Informatics. To induce atherosclerosis, we fed mice initially a chow diet and then an atherogenic high-fat diet[35] when they were 8–10 weeks old. Only female mice were studied because the *Ath1* phenotype was found in females[36–38]. All animal protocols were approved by the Jackson Laboratory Animal Care and Use Committee.

Evaluation of aortic atherosclerotic lesions in mice. The phenotype of *Ath1* was found by measuring the diet-induced atherosclerotic lesion size at aortic roots[36–38], and we measured the same phenotype in this study. After the mice had been fed an atherogenic diet for 10–13 weeks, they were killed by cervical dislocation, and their hearts and ascending aortas were removed and fixed in 4% formaldehyde. We measured atherosclerotic lesions on the aortic root of each mouse as described previously[39]. The lesion size for each mouse was determined by averaging the lesion sizes of five sections and was expressed as mean μm^2 per section.

Plasma lipid measurement in mice. We fasted the mice for 4 h and then collected blood from their retro-orbital plexus into tubes containing EDTA. We separated plasma by centrifuging the samples for 5 min at 1,500 r.p.m. at 4 °C. We measured plasma total cholesterol, HDL cholesterol (measured after precipitating and removing APOB-containing lipoproteins) and triglyceride levels in a chemical analyzer (Beckman Synchron CX5 Delta) and calculated

non-HDL (very-low-density lipoprotein and LDL) cholesterol levels by subtracting HDL cholesterol levels from total cholesterol levels.

Mouse DNA isolation and genotyping. We prepared genomic DNA from mouse tail tips as previously described[40]. PCR genotyping of *Prdx6*$^{-/-}$ mice[5] and *Tnfsf4*$^{-/-}$ mice[34] has been detailed. We genotyped *Apoe* in *Apoe*-targeted mutant (*Apoe*$^{-/-}$) mice using the protocol provided by the supplier.

Gene sequencing. We obtained genomic DNA of B6 and C3H strains from DNA Resources at The Jackson Laboratory. To sequence the mouse candidate genes for *Ath1*, we amplified each exon with PCR and sequenced the PCR products using Big Dye Terminator Cycle Sequencing Chemistry and the ABI 3700 Sequence Detection System.

We sequenced human *TNFSF4* in the genomic DNA from whole blood of 20 healthy subjects. We amplified the three exons of *TNFSF4* with PCR and used the PCR products as templates for further amplifications as part of the Taq DyeDeoxy terminator cycle-sequencing system (Perkin-Elmer Corp.). The sequences of the PCR primers are provided in **Supplementary Table 4** online.

RNA preparation and quantitative real-time PCR. We preserved tissues in RNAlater (Ambion) before extracting total RNA using RNeasy Mini Kit (Qiagen)[40]. We carried out quantitative real-time PCR using the ABI Prism 7000 Sequence Detection System (PE Applied Biosystems) as previously described[40]. We designed primers using the primer design software Primer Express 2.0 (PE Applied Biosystems). To ensure that the primers amplified a unique and desired cDNA segment, the forward and reverse primers for each pair of primers are located on different exons, each potential pair of primers was checked in the BLAST program in Ensembl database and Celera Discovery System, there was only one PCR product from each pair of primers as seen by electrophoresis, and the product was sequenced to confirm that the correct gene was amplified. We normalized the mRNA expression of each gene to the copies of β-actin (*Actb*) mRNA from the same sample. The primer sequences for amplifying *Tnfsf4*, *Tnfsf6* and β-actin cDNA are shown in **Supplementary Table 4** online. We carried out real-time PCR assays in triplicate.

Immunohistochemistry. We generated rabbit IgG antibody to mouse OX40L by repeatedly immunizing rabbits with a synthetic OX40L peptide (LDENLENGSRPRFKWKKTLRC). We obtained antisera two weeks after the fourth immunization. We affinity-purified the IgG fractions against the peptide. We tested the specificity of the antibodies by western blotting: the antibody reacted with a 34-kDa membrane protein from the spleen of a B6 mouse but not with any proteins from a *Tnfsf4*$^{-/-}$ mouse. We embedded mouse tissues in paraffin and sectioned them after fixing them in Bouin's fixative. We stained 4-μm sections with hemotoxylin and eosin. For immunohistochemistry, we blocked endogenous peroxidase activity in the sectioned tissues with 0.3% H_2O_2 and blocked nonspecific binding sites with nonimmune goat serum. We then applied rabbit antibody to mouse OX40L. We detected specific binding using biotinylated secondary antibody and avidin–biotin–horseradish peroxidase complex (Santa Cruz) and diamino benzidine as a substrate. We counterstained nuclei with hemotoxylin.

Human subjects: SCARF project. A total of 383 individuals with myocardial infarction before age 60 were genotyped. They were recruited from those admitted to the coronary care units of the Danderyd, Karolinska and Norrtälje Hospitals in Stockholm County, Sweden, within the framework of the SCARF project, between January 1996 and December 2000 (ref. 41). For each eligible post-infarction individual, a sex- and age-matched control person was recruited from the general population of the same catchment area. Three months after the index cardiac event in an individual, both the individual and a control subject underwent a structured interview and blood sampling, and the affected individuals in two of the three hospitals were offered routine coronary angiography. A total of 252 affected individuals (66%) went through routine invasive evaluation with quantitative coronary angiography. All individuals were interviewed and examined to exclude a history of diabetes mellitus type 1, severely impaired renal functions (serum creatinine >200 μmol l^{-1}), systemic diseases (such as rheumatoid arthritis, systemic lupus erytematosus, inflammatory bowel disease and chronic hepatitis), alcohol abuse or other forms of addiction, and chronic psychiatric illness.

Human subjects: SHEEP. SHEEP constituted a second human population consisting of 2,246 men and women who were admitted to hospital for treatment of a first-time myocardial infarction and 3,206 unaffected controls[42]. The subjects, aged 45–70, were all Swedish citizens. Male cases were identified between 1992 and 1993 and female cases between 1992 and 1994. This report is restricted to the 1,213 cases that survived 28 days after their myocardial infarction and had no further events before blood sampling and the 1,561 matched controls. One control per case was randomly selected from the Stockholm County population registry within 2 d of the case event, after stratification for age (5-y intervals), sex and residential area. Five control candidates per case were sampled at the same time so that nonrespondent controls could be replaced by another candidate who belonged to the study base at the case incident. Occasionally, both the initial and a substitute control were included owing to late reply of the initial control. With this procedure (case/referent design), more controls than cases were included. Blood samples were collected approximately three months after the acute event in the cases to allow them to achieve a stable metabolic state. All subjects gave informed consent to their participation in the studies, the protocols of which had been approved by the ethics committee of the Karolinska Hospital.

Established risk factors and severity of coronary artery disease. We carried out laboratory analyses of established risk factors as previously described[43]. We carried out coronary angiography either during the initial admission, if needed for clinical reasons, or three months after the onset of myocardial infarction otherwise. We then analyzed angiograms in 15 coronary segments[44] by the Medis system (MEDIS medical imaging systems) for quantitative coronary angiography. We measured the reference diameter, minimal lumen diameter, percent diameter stenosis, mean segment diameter, segment length, plaque area, segment area and number of significant (>50%) stenoses in each segment.

SNP genotyping and haplotype analysis in humans. We retrieved the polymorphisms of the genes in the *Ath1* human homologous region from the SNP database (build 116) of the National Center for Biotechnology Information. All participants were genotyped for the polymorphisms listed in **Table 2.** We amplified DNA using primer pairs with one 5′ end biotinylated (**Supplementary Table 4** online). We captured the amplification products on streptavidin-coated magnetic beads (Dynabeads, Dynal A.S.), denatured them and then washed them. We added pyrosequencing primer (**Supplementary Table 4** online) and analyzed the mix as previously described[45]. We carried out pyrosequencing using the PSQ96 SQA Reagent Kit and Sample Preparation Kit 10x96. We determined genotypes using the PSQ SNP Software version 1.3 (Pyrosequencing AB). We carried out haplotype analysis using the HAPLOTYPER program[46].

Statistical analysis. We carried out statistical analyses using the StatView or SAS version 8.0 software (SAS). Continuous data are expressed as means ± s.e.m. We estimated allele frequencies by the gene counting method and tested them for the presence of Hardy-Weinberg equilibrium using the χ^2 method. We also used the χ^2 test to compare the distributions of genotypes between cases and controls and to compare categorical data between groups. We tested the differences in continuous variables between groups by analysis of variance with the Scheffe F test as a post-hoc test. To obtain a normal distribution before carrying out statistical computations and significance testing, we log-transformed all skewed variables. We calculated pairwise linkage disequilibrium coefficients for the polymorphisms in the *TNFSF4* locus with the EMLD program developed by Q. Huang (Department of Epidemiology, MD Anderson Cancer Center, University of Texas). We estimated haplotype frequencies using the HAPLOTYPER program[46], which uses a bayesian algorithm. We calculated odds ratios with 95% confidence intervals, as estimates of the relative risk, using logistic regression. Adjustments were made for age, gender, residential area, LDL cholesterol, HDL cholesterol, triglycerides, body mass index and smoking.

We used Student's *t*-test to compare the mRNA expression levels, the size of the diet-induced atherosclerotic lesions and plasma lipid levels between the mutant mice and their respective controls. All values are expressed as mean ± s.e.

URLs. See http://request.mdacc.tmc.edu/~qhuang/Software/pub.htm for the EMLD program. The Celera Discovery System is available at http://myscience.

appliedbiosystems.com/. The Ensembl database is available at http://www.ensembl.org/. Mouse Genome Informatics is available at http://www.informatics.jax.org/.

Note: Supplementary information is available on the Nature Genetics website.

ACKNOWLEDGMENTS

We thank C. McFarland for technical assistance and R. Lambert for helping to prepare the manuscript. This study was supported by AstraZeneca (Sweden), grants from the US National Institutes of Health and grants from the Swedish Heart-Lung Foundation, the Swedish Medical Research Council, the Torsten and Ragnar Söderberg foundation, AFA insurance, the Stockholm County Council, the Wallenberg Consortium North, the Swedish Society for Medical Research and the Karolinska Institute.

COMPETING INTERESTS STATEMENT

The authors declare that they have no competing financial interests.

Received 15 November 2004; accepted 10 January 2005
Published online at http://www.nature.com/naturegenetics/

1. Paigen, B., Morrow, A., Brandon, C., Mitchell, D. & Holmes, P. Variation in susceptibility to atherosclerosis among inbred strains of mice. *Atherosclerosis* **57**, 65–73 (1985).
2. Paigen, B. *et al.* Ath-1, a gene determining atherosclerosis susceptibility and high density lipoprotein levels in mice. *Proc. Natl. Acad. Sci. USA* **84**, 3763–3767 (1987).
3. Paigen, B., Albee, D., Holmes, P.A. & Mitchell, D. Genetic analysis of murine strains C57BL/6J and C3H/HeJ to confirm the map position of Ath-1, a gene determining atherosclerosis susceptibility. *Biochem. Genet.* **25**, 501–511 (1987).
4. Phelan, S.A., Beier, D.R., Higgins, D.C. & Paigen, B. Confirmation and high resolution mapping of an atherosclerosis susceptibility gene in mice on Chromosome 1. *Mamm. Genome* **13**, 548–553 (2002).
5. Wang, X. *et al.* Mice with targeted mutation of peroxiredoxin 6 develop normally but are susceptible to oxidative stress. *J. Biol. Chem.* **278**, 25179–25190 (2003).
6. Phelan, S.A., Wang, X., Wallbrandt, P., Forsman-Semb, K. & Paigen, B. Overexpression of Prdx6 reduces H2O2 but does not prevent diet-induced atherosclerosis in the aortic root. *Free Radic. Biol. Med.* **35**, 1110–1120 (2003).
7. Wang, X. *et al.* Peroxiredoxin 6 deficiency and atherosclerosis susceptibility in mice: significance of genetic background for assessing atherosclerosis. *Atherosclerosis* **177**, 61–70 (2004).
8. Geng, Y.J. Biologic effect and molecular regulation of vascular apoptosis in atherosclerosis. *Curr. Atheroscler. Rep.* **3**, 234–242 (2001).
9. Weinberg, A.D. OX40: targeted immunotherapy–implications for tempering autoimmunity and enhancing vaccines. *Trends Immunol.* **23**, 102–109 (2002).
10. Hansson, G.K., Libby, P., Schonbeck, U. & Yan, Z.Q. Innate and adaptive immunity in the pathogenesis of atherosclerosis. *Circ. Res.* **91**, 281–291 (2002).
11. Shi, W. *et al.* Genetic backgrounds but not sizes of atherosclerotic lesions determine medial destruction in the aortic root of apolipoprotein E-deficient mice. *Arterioscler. Thromb. Vasc. Biol.* **23**, 1901–1906 (2003).
12. Mehrabian, M. *et al.* Identification of 5-lipoxygenase as a major gene contributing to atherosclerosis susceptibility in mice. *Circ. Res.* **91**, 120–126 (2002).
13. Emeson, E.E., Shen, M.L., Bell, C.G. & Qureshi, A. Inhibition of atherosclerosis in CD4 T-cell-ablated and nude (nu/nu) C57BL/6 hyperlipidemic mice. *Am. J. Pathol.* **149**, 675–685 (1996).
14. Nakai, Y. *et al.* Natural killer T cells accelerate atherogenesis in mice. *Blood* **104**, 2051–2059 (2004).
15. Major, A.S., Fazio, S. & Linton, M.F. B-lymphocyte deficiency increases atherosclerosis in LDL receptor-null mice. *Arterioscler. Thromb. Vasc. Biol.* **22**, 1892–1898 (2002).
16. Caligiuri, G., Nicoletti, A., Poirier, B. & Hansson, G.K. Protective immunity against atherosclerosis carried by B cells of hypercholesterolemic mice. *J. Clin. Invest.* **109**, 745–753 (2002).
17. Reardon, C.A. *et al.* Effect of immune deficiency on lipoproteins and atherosclerosis in male apolipoprotein E-deficient mice. *Arterioscler. Thromb. Vasc. Biol.* **21**, 1011–1016 (2001).
18. Song, L., Leung, C. & Schindler, C. Lymphocytes are important in early atherosclerosis. *J. Clin. Invest.* **108**, 251–259 (2001).
19. Dansky, H.M., Charlton, S.A., Harper, M.M. & Smith, J.D. T and B lymphocytes play a minor role in atherosclerotic plaque formation in the apolipoprotein E-deficient mouse. *Proc. Natl. Acad. Sci. USA* **94**, 4642–4646 (1997).
20. Geng, Y.J. & Libby, P. Progression of atheroma: a struggle between death and procreation. *Arterioscler. Thromb. Vasc. Biol.* **22**, 1370–1380 (2002).
21. Yang, J. *et al.* Endothelial overexpression of Fas ligand decreases atherosclerosis in apolipoprotein E-deficient mice. *Arterioscler. Thromb. Vasc. Biol.* **24**, 1466–1473 (2004).
22. Aprahamian, T. *et al.* Impaired clearance of apoptotic cells promotes synergy between atherogenesis and autoimmune disease. *J. Exp. Med.* **199**, 1121–1131 (2004).
23. Schneider, D.B. *et al.* Expression of Fas ligand in arteries of hypercholesterolemic rabbits accelerates atherosclerotic lesion formation. *Arterioscler. Thromb. Vasc. Biol.* **20**, 298–308 (2000).
24. Kotani, A., Hori, T., Matsumura, Y. & Uchiyama, T. Signaling of gp34 (OX40 ligand) induces vascular endothelial cells to produce a CC chemokine RANTES/CCL5. *Immunol. Lett.* **84**, 1–7 (2002).
25. Kawai, T. *et al.* Selective diapedesis of Th1 cells induced by endothelial cell RANTES. *J. Immunol.* **163**, 3269–3278 (1999).
26. Welch, C.L. *et al.* Localization of atherosclerosis susceptibility loci to chromosomes 4 and 6 using the Ldlr knockout mouse model. *Proc. Natl. Acad. Sci. USA* **98**, 7946–7951 (2001).
27. Hauser, E.R. *et al.* A genomewide scan for early-onset coronary artery disease in 438 families: the GENECARD Study. *Am. J. Hum. Genet.* **75**, 436–447 (2004).
28. Wang, Q. *et al.* Premature myocardial infarction novel susceptibility locus on chromosome 1p34-36 identified by genomewide linkage analysis. *Am. J. Hum. Genet.* **74**, 262–271 (2004).
29. Abiola, O. *et al.* The nature and identification of quantitative trait loci: a community's view. *Nat. Rev. Genet.* **4**, 911–916 (2003).
30. Stary, H.C. *et al.* A definition of advanced types of atherosclerotic lesions and a histological classification of atherosclerosis. A report from the Committee on Vascular Lesions of the Council on Arteriosclerosis, American Heart Association. *Circulation* **92**, 1355–1374 (1995).
31. Edfeldt, K. *et al.* Association of hypo-responsive toll-like receptor 4 variants with risk of myocardial infarction. *Eur. Heart J.* **25**, 1447–1453 (2004).
32. Paigen, B., Holmes, P.A., Mitchell, D. & Albee, D. Comparison of atherosclerotic lesions and HDL-lipid levels in male, female, and testosterone-treated female mice from strains C57BL/6, BALB/c, and C3H. *Atherosclerosis* **64**, 215–221 (1987).
33. Sugamura, K., Ishii, N. & Weinberg, A.D. Therapeutic targeting of the effector T-cell co-stimulatory molecule OX40. *Nat. Rev. Immunol.* **4**, 420–431 (2004).
34. Murata, K. *et al.* Impairment of antigen-presenting cell function in mice lacking expression of OX40 ligand. *J. Exp. Med.* **191**, 365–374 (2000).
35. Nishina, P.M., Verstuyft, J. & Paigen, B. Synthetic low and high fat diets for the study of atherosclerosis in the mouse. *J. Lipid Res.* **31**, 859–869 (1990).
36. Paigen, B. *et al.* Ath-1, a gene determining atherosclerosis susceptibility and high density lipoprotein levels in mice. *Proc. Natl. Acad. Sci. USA* **84**, 3763–3767 (1987).
37. Paigen, B., Mitchell, D., Holmes, P.A. & Albee, D. Genetic analysis of strains C57BL/6J and BALB/cJ for Ath-1, a gene determining atherosclerosis susceptibility in mice. *Biochem. Genet.* **25**, 881–892 (1987).
38. Paigen, B., Albee, D., Holmes, P.A. & Mitchell, D. Genetic analysis of murine strains C57BL/6J and C3H/HeJ to confirm the map position of Ath-1, a gene determining atherosclerosis susceptibility. *Biochem. Genet.* **25**, 501–511 (1987).
39. Paigen, B., Morrow, A., Holmes, P.A., Mitchell, D. & Williams, R.A. Quantitative assessment of atherosclerotic lesions in mice. *Atherosclerosis* **68**, 231–240 (1987).
40. Wang, X. *et al.* Using advanced intercross lines for high-resolution mapping of HDL cholesterol quantitative trait loci. *Genome. Res.* **13**, 1654–1664 (2003).
41. Eriksson, P. *et al.* Human evidence that the cystatin C gene is implicated in focal progression of coronary artery disease. *Arterioscler. Thromb. Vasc. Biol.* **24**, 551–557 (2004).
42. Reuterwall, C. *et al.* Higher relative, but lower absolute risks of myocardial infarction in women than in men: analysis of some major risk factors in the SHEEP study. The SHEEP Study Group. *J. Intern. Med.* **246**, 161–174 (1999).
43. Boquist, S. *et al.* Alimentary lipemia, postprandial triglyceride-rich lipoproteins, and common carotid intima-media thickness in healthy, middle-aged men. *Circulation* **100**, 723–728 (1999).
44. Austen, W.G. *et al.* A reporting system on patients evaluated for coronary artery disease. Report of the Ad Hoc Committee for Grading of Coronary Artery Disease, Council on Cardiovascular Surgery, American Heart Association. *Circulation* **51**, 5–40 (1975).
45. Ronaghi, M., Uhlen, M. & Nyren, P. A sequencing method based on real-time pyrophosphate. *Science* **281**, 363–365 (1998).
46. Niu, T., Qin, Z.S., Xu, X. & Liu, J.S. Bayesian haplotype inference for multiple linked single-nucleotide polymorphisms. *Am. J. Hum. Genet.* **70**, 157–169 (2002).

THE JOURNAL OF BIOLOGICAL CHEMISTRY
Vol. 280, No. 11, Issue of March 18, pp. 10468–10477, 2005
Printed in U.S.A.

Hrs, a Mammalian Master Molecule in Vesicular Transport and Protein Sorting, Suppresses the Degradation of ESCRT Proteins Signal Transducing Adaptor Molecule 1 and 2*

Received for publication, August 31, 2004, and in revised form, January 7, 2005
Published, JBC Papers in Press, January 7, 2005, DOI 10.1074/jbc.M409969200

Hideyuki Kobayashi‡§, Nobuyuki Tanaka‡¶, Hironobu Asao‖, Shigeto Miura‡, Masanao Kyuuma‡, Kayoko Semura‡, Nobuhisa Ishii and Kazuo Sugamura‡**

*From the ‡Department of Microbiology and Immunology, Tohoku University Graduate School of Medicine, 2-1 Seiryo-machi, Aoba-ku, Sendai, 980-8575, Japan, ‖Department of Immunology, Yamagata University School of Medicine, 2-2-2 Iida-Nishi, Yamagata, 990-9585, Japan, and **First Department of Urology, Toho University School of Medicine, 6-11-1 Omori-nishi, Ota-ku, Tokyo, 143-8541, Japan*

The degradation and sorting of cytoplasmic and cell-surface proteins are crucial steps in the control of cellular functions. We previously identified three mammalian Vps (vacuolar protein sorting) proteins, Hrs (hepatocyte growth factor-regulated tyrosine kinase substrate) and signal transducing adaptor molecule (STAM) 1 and -2, which are tyrosine-phosphorylated upon cytokine/growth factor stimulation. Hrs and the STAMs each contain a ubiquitin-interacting motif and through formation of a complex are involved in the vesicle transport of early endosomes. To explore the mechanism and cellular function of this complex in mammalian cells, we established an Hrs-defective fibroblastoid cell line ($hrs^{-/-}$); embryos with this genotype died *in utero*. In the $hrs^{-/-}$ cells only trace amounts of STAM1 and STAM2 were detected. Introduction of wild-type Hrs or an Hrs mutant with an intact STAM binding domain (Hrs-dFYVE) fully restored STAM1 and STAM2 expression, whereas mutants with no STAM binding ability (Hrs-dC2, Hrs-dM) failed to express the STAMs. This regulated control of STAM expression by Hrs was independent of transcription. Interestingly, STAM1 degradation was mediated by proteasomes and was partially dependent on the ubiquitin-interacting motif of STAM1. Revertant Hrs expression in $hrs^{-/-}$ cells not only led to the accumulation of ubiquitinated proteins, including intracytoplasmic vesicles, but also restored STAM1 levels in early endosomes and eliminated the enlarged endosome phenotype caused by the absence of Hrs. These results suggest that Hrs is a master molecule that controls in part the degradation of STAM1 and the accumulation of ubiquitinated proteins.

Membrane traffic is a dynamic process that is responsible for the maintenance of cellular metabolism, stress response, down-regulation of cell-surface molecules, and signal transduction. Cell-surface molecules, including growth factor receptors that bind to specific ligands or macromolecules, are internalized from the cell surface into membrane compartments called endosomes. Although some cargos are pinched off in recycling endosomes to be sent back to the cell surface, other receptors and molecules are pinched off into endosomes that form multivesicular bodies (MVB).[1] As the maturation step proceeds, early endosomes become acidic to form late endosomes, which then fuse with acidic compartments called lysosomes, which contain many acidic proteases. Although it has not been clear how receptors that have captured their ligands are recognized and sequestered into the endocytic vesicles, a growing body of evidence suggests the involvement of monoubiquitin modification and implicates the intracytoplasmic region of the receptors (1).

The identification of vacuolar protein sorting (Vps) mutants has permitted genetic analyses in yeast to identify the proteins that make up the core machinery for MVB formation. The functional loss of Vps proteins results in deformed MVBs with unusually enlarged vesicles, called "class E" compartments, and defective vesicular trafficking. At present, 17 Vps genes are known; they are genetically categorized into four kinds of endosomal sorting complexes required for transport (ESCRT), ESCRT-0, I, II, and III. One of the ESCRT proteins involved in MVB formation is yeast Vps27. Vps27, along with Hse1, acts in an ESCRT-0 complex upstream of ESCRT-I to assist in protein sorting (2).

In studies to find molecules involved in cytokine/growth factor signaling, we identified Hrs, STAM1, and STAM2 (3–5). Hrs is a mammalian orthologue of yeast Vps27, and STAM1 and STAM2 are mammalian counterparts of yeast Hse1. We as well as others previously reported that cytokines and growth factors such as interleukin 2, granulocyte-macrophage colony-stimulating factor, hepatocyte growth factor, platelet-derived growth factor, and epidermal growth factor induce the tyrosine phosphorylation of Hrs and the STAMs (3, 4, 6). The rapid kinetics of their phosphorylations prompted us to look for the functions of these molecules, which are immediately downstream of the receptors. Hrs possesses several functional domains, including a FYVE finger domain, which binds specifi-

* This work was supported in part by a grant-in-aid for Scientific Research from the Japan Society for the Promotion of Science, a grant-in-aid from the 21st Century Center of Excellence (COE) Program Special Research Grant, and a grant-in-aid for Scientific Research on Priority Areas from the Ministry of Education, Science, Sports, and Culture of the Japanese Government. The costs of publication of this article were defrayed in part by the payment of page charges. This article must therefore be hereby marked "*advertisement*" in accordance with 18 U.S.C. Section 1734 solely to indicate this fact.

§ Research Fellow of the Japan Society for the Promotion of Science.
¶ To whom correspondence should be addressed. Tel.: 81-22-717-8096; Fax: 81-22-717-8097; E-mail: n-tanaka@mail.tains.tohoku.ac.jp.

[1] The abbreviations used are: MVB, multivesicular bodies; Vps, vacuolar protein sorting; Hrs, hepatocyte growth factor-regulated tyrosine kinase substrate; STAM1 and STAM2, signal transducing adaptor molecule 1 and 2; UIM, ubiquitin-interacting motif; ESCRT, endosomal sorting complexes required for transport; VHS, Vps27-Hrs-STAM; ITAM, immunoreceptor tyrosine-based activation motif; RT, reverse transcription; MEF, mouse embryonic fibroblastoid; HA, hemagglutinin; E3, ubiquitin ligase; Ub, ubiquitin.

cally to phosphatidylinositol 3-phosphate and is important for membrane anchoring, and a clathrin binding domain, required for membrane-coated vesicle binding (7–11). Hrs also contains an N-terminal VHS (Vps27-Hrs-STAM) domain and a ubiquitin-interacting motif (UIM). The overexpression of Hrs, but not of a UIM deletion mutant, inhibits the recycling of a ubiquitin-fused transferrin receptor, suggesting a role for Hrs-UIM in vesicular transport (12). Furthermore, an accumulation of ligand-activated epidermal growth factor receptors within early endosomes is observed in cells overexpressing Hrs, suggesting the involvement of Hrs in ubiquitinated protein sorting (11, 13–15).

After the identification of STAM1 and STAM2 (EAST/Hbp), two closely related molecules, we showed that their roles in intracellular cytokine/growth factor signaling included induction of the proto-oncogene *c-myc* (3, 5, 16–18). The STAMs have a unique structure, including a VHS, a UIM, an Src homology 3 (SH3) domain, and an ITAM (immunoreceptor tyrosine-based activation motif) (3, 5). We and others reported that the ITAMs of STAM1 and STAM2 associate with Hrs through its second coiled-coil (CC2) domain (4). Like its binding partner, STAM2 binds directly to ubiquitins (19). Both Hrs and the STAMs bind Eps15, and therefore, all these molecules seem to participate in the sorting of ubiquitinated proteins into the MVB pathway (19).

To further characterize the function of the mammalian STAM-Hrs complexes in MVB formation and/or protein sorting, we established Hrs-deficient fibroblastoid cell lines. The results of introducing wild-type or a mutant Hrs into these cells suggested a novel function for Hrs in regulating the fate of ubiquitinated proteins. We demonstrate here that Hrs controls the STAM protein stability. Our demonstration of the STAM relationship with ubiquitinated proteins provides insight into how their UIM domain functions in protein sorting.

EXPERIMENTAL PROCEDURES

Targeted Disruption of hrs in Vivo—Genomic clones of the mouse *hrs* gene were isolated from a λFixIImouse 129/Sv genomic library (Stratagene). A targeting construct for *hrs* was designed to replace a 0.6-kilobase (HindIII-HindIII) genomic fragment encompassing exon 6, flanked by 3.2-kilobase (XbaI-XbaI) and 3.0-kilobase (EcoRI-XbaI) genomic sequences (Fig. 1*A*). A pGK-neo cassette flanked by a pair of loxP sequences and a diphtheria toxin A-chain (DT) gene cassette without a polyadenylation site were inserted into the construct to allow further positive/negative selection. The construct was linearized and transferred into 129/Sv-derived J1 ES cells by electroporation, and G418-resistant colonies were picked (20–22). The occurrence of homologous recombination events for the *hrs* allele was examined by Southern hybridization using a 1.8-kilobase *hrs* genomic fragment (XbaI-BamHI) as the probe (Fig. 1*B*). The targeted *hrs* loxP-flanked (floxP) ES clone was confirmed to have a normal number of chromosomes and was injected into C57BL/6 blastocysts. The blastocysts were then transferred into foster mothers to obtain chimeric mice. By crossing the chimeras with C57BL/6 mice we obtained F_1 heterozygous mice carrying the floxP allele. The genotypes were confirmed by both genomic PCR and Southern blot analyses (data not shown). The F_1 heterozygous mice were intercrossed, but the genotyping of more than 100 offspring showed that no viable $hrs^{floxP/floxP}$ mice were produced. To identify $hrs^{floxP/floxP}$ embryos *in utero*, the genotypes of living embryos were determined using yolk sac DNA (23). The following oligonucleotide primers were used: Hrs-1650F (primer A), 5′-GAGTGAGGAGGCGGTGTTCCCTAAACCTTG-3′; Hrs-1953R (primer B), 5′-AACATATACTGCTGGCAAAGCATCCATACA-3′; Hrs-CKO1787R (primer C), 5′-TATAGCATACATTATACGAAGTTATGTCGA-3′. PCR was carried out by initial denaturation at 94 °C for 5 min followed by 35 cycles of 30 s at 94 °C, 30 s at 60 °C, and 30 s at 72 °C. The wild-type and mutant alleles gave rise to PCR-amplified fragments of 330 and 160 bp, respectively (Fig. 1*C*).

Establishment of hrs-deficient and hrs-mutant Embryonic Fibroblastoid Cell Lines—Primary fibroblastoid cells derived from E9.5 $hrs^{floxP/floxP}$ mouse embryos were obtained through timed-breeding experiments, as described previously (24). Cells were stably immortalized by transfecting them with pEF321-T, an SV40 large T-antigen expression plasmid. Deletion of the floxP fragment was performed by transient transfection with pCXN2-Cre, a Cre-recombinase expression construct. The presence in cells of the *hrs* deletion ($hrs\Delta/\delta$) was verified by PCR. The following oligonucleotide primers were used: neo2760F (primer D), 5′-CTTGGGTGGAGAGGCTATTC-3′; neo3030R (primer E), 5′-AGGTGAGATGACAGGAGATC-3′; Hrs-1650F (primer A), 5′-GAGTGAGGAGGCGGTGTTCCCTAAACCTTG-3′; Hrs-CKO4108R (primer F), 5′-ATCACATTTCCCTCCCCAGTGCTTTCAAAC-3′. Limiting dilution and subsequent cloning were used to establish HRSd, an immortalized fibroblastoid cell line carrying the $hrs^{\delta/\delta}$ genotype (Fig. 1*E*). HRSw, HRSdC2, HRSdFYVE, and HRSdM were HRSd sublines stably transformed with expression vectors for wild-type Hrs and for the dC2, dFYVE, and dM Hrs mutants, respectively. The expression of the wild-type or mutated Hrs proteins in these clones was confirmed by Western blotting.

Reverse-transcription (RT)-PCR—RT-PCR was carried out with the total RNA derived from HRSd and MEFw cells. The total RNA was prepared with TRIzol Reagent (Invitrogen) and subjected to first-strand synthesis using the SuperScript III first-strand synthesis system (Invitrogen). PCRs were performed with a series of 3-fold-diluted templates to amplify the *hrs* and *β-actin* cDNAs. The primer set for *hrs* was designed to amplify a coding region within the N-terminal VHS domain. The primers used were as follows: Hrs-Exon 1 sense, 5′-TTCGAGCGTCTCCTAGACAAAGC-3′; Hrs-Exon 3 antisense, 5′-CATATTTTGCTTGTGTGTCCCCC-3′; β-actin sense, 5′-CCACTGCCACATCCTCTTC-3′; β-actin antisense: 5′-CATCTGCTGGAAGGTGGAC-3′

Plasmids—pCXN2-Hrs, pCXN2-STAM1-V5, and pCXN2-STAM2-V5 were expression plasmids for wild-type Hrs, STAM1, and STAM2, respectively. Expression vectors for the mutated Hrs, Hrs-dC2, Hrs-dFYVE, and Hrs-dM were described previously (4, 5, 16, 25, 26). An expression plasmid for DsRed1-fused Eps15 (DsRed1-Eps15) was generated by ligating a PCR-amplified human Eps15 cDNA into pDSRed1-C1 (Clontech). A newly developed expression plasmid for HrsL265E (Hrs-mUIM) was generated using a PCR fragment of human Hrs carrying a point mutation at amino acid 265 (27) ligated into pCXN2. The expression plasmid for V5-tagged STAM1 with point mutations at leucines 176, 182, and 184 that caused them to be substituted with alanine (STAM1-mUIM-V5) was generated by ligating the PCR fragment of wild-type human STAM1 with point mutations at amino acids 176, 182, and 184 into pCXN2. The SV40 large T-antigen expression plasmid, pEF321-T, was a kind gift from Dr. M. Obinata (Tohoku University), and the expression plasmid for ubiquitin, pcDNA3-HA-Ub, was a kind gift from Dr. K. Miyazono (Tokyo University) (28). FLAG-tagged ubiquitin, p3XFLAG-Ub, was generated by PCR-based cloning of human ubiquitin into the p3XFLAG-CMV-10 vector (Sigma).

Cell Culture—HRSd and HRSd sublines transfected with wild-type Hrs or Hrs mutants were cultured in Dulbecco's modified Eagle's medium supplemented with 10% fetal calf serum and antibiotics under 7% CO_2 in a humidified incubator. To transfect the cells with plasmid DNAs, FuGENE™ 6 transfection reagent (Roche Applied Science) was used according to the manufacturer's protocol. Where indicated lactacystin (Kyowa Medex) and E-64-d (Peptide Institute, Inc.) were added to the cell culture to a final concentration of 10 and 100 μM, respectively.

Immunoprecipitation and Immunoblots—Immunoprecipitation and immunoblotting were carried out as described previously (4). In brief, cells were lysed in Nonidet P-40 lysis buffer (1% Nonidet P-40, 40 mM Tris-HCl (pH 7.5), 150 mM NaCl, 2 mM EDTA, 1 mM Na_3VO_4, 1 mM phenylmethylsulfonyl fluoride, and 20 μg/ml aprotinin). The cell lysates were precleared of cellular debris by centrifugation (10,000 × *g*) for 20 min at 4 °C and were then subjected to immunoprecipitation with antibodies immobilized on protein A-Sepharose beads (Amersham Biosciences) at 4 °C overnight. For this assay rabbit anti-Hrs polyclonal antibodies (4) and anti-ubiquitin (Santa Cruz), anti-STAM1 (TUS-1) (29), anti-STAM2 (ST2–2) (5), and anti-V5 monoclonal antibodies (Invitrogen) were used. The immunoprecipitates were then separated by SDS-PAGE and transferred onto polyvinylidene difluoride membranes (Millipore). After being blocked with 5% nonfat milk in Tris-buffered saline containing 0.1% Tween 20, the membranes were probed with the indicated primary antibodies. After another wash, the membranes were probed with horseradish peroxidase-conjugated secondary antibodies (Cell Signaling). Signals were visualized by the ECL detection system (Amersham Biosciences), and digital images were collected by a Lumi-Imager F1 (Roche Applied Science). For degradation assays, the cells were cultured in the presence of 25 μg/ml cycloheximide (Wako) for the period indicated, and the cell lysates from these cultures were analyzed by Western blotting.

Northern Blots—Northern blot analyses were performed as described

previously (29). In brief, total RNA was prepared using TRIzol Reagent (Invitrogen). Twenty micrograms of total RNA was fractionated by electrophoresis in a 0.8% agarose gel containing formaldehyde. The separated RNAs were then transferred onto Hybond-N$^+$ membranes (Amersham Biosciences) in 10 x SSC. After UV-cross-linking, the membranes were subjected to prehybridization and hybridization in a solution containing 0.5 M sodium phosphate (pH 7.2), 1 mM EDTA, and 7% SDS at 65 °C. A probe prepared by radiolabeling with [α-^{32}P]dCTP using a Random Prime-DNA labeling kit (Takara Shuzo Co.) was added, and hybridization was carried out overnight. Membranes were then extensively washed with a washing buffer (2× SSC (1× SSC = 0.15 M NaCl and 0.015 M sodium citrate), 0.1% SDS) at 65 °C, and the signals were visualized with a Bio-Image Analyzer, FLA-2000 (Fuji Film). The probes used to detect murine *stam1*, *stam2*, and glyceraldehyde-3-phosphate dehydrogenase (*gapdh*) mRNAs were described elsewhere (29, 30).

Immunofluorescence Microscopy and Immunostaining—Cells were seeded into 35-mm glass-bottomed dishes (MatTek Co.) at a density of 1×10^5 cells/dish 1 day before the transfection. DsRed1-Eps15 was then introduced as described above. After 48 h, the cells were washed twice with phosphate-buffered saline, fixed with 4% paraformaldehyde for 15 min, permeabilized for 10 min with phosphate-buffered saline containing 0.1% Triton X-100, and then blocked for 30 min with phosphate-buffered saline containing 10% fetal calf serum and 0.1% Triton X-100. For immunostaining, the fixed samples were incubated with the indicated primary antibodies, washed 3 times, and further probed with the secondary antibodies (anti-rabbit, -mouse, and -goat IgG antibodies conjugated with Alexa 488, Alexa 594, and Alexa 350, respectively (Molecular Probes)). The microscopic images were examined using the Leica DMIRBE microscope system with a PL FLUOTAR 100×/1.30–0.60 oil immersion objective.

Metabolic Labeling of Cellular Proteins—For pulse-chase experiments, HRSd and 293T cells that had been transiently transfected with the indicated plasmids using FuGENE^{TM} 6 were radiolabeled with the Pro-mix $_L$-[^{35}S] in Vitro Cell Labeling Mix at a concentration of 100 μCi/ml (Amersham Biosciences) in Met/Cys-free Dulbecco's modified Eagle's medium (Invitrogen) supplemented with 10% fetal calf serum that had been predialyzed against phosphate-buffered saline for 30 min. At the end of the pulse-labeling period, the cells were washed and chased for the indicated times in complete Dulbecco's modified Eagle's medium supplemented with methionine and cysteine. Cells were collected by centrifugation, and the lysates made from them were subjected to further immunoprecipitation assays. Radioactivity was visualized and analyzed using Science Lab 2001 Image Gauge Version 4.0 software (Fuji Film).

RESULTS

Establishment of hrs-deficient Cell Lines by Gene Targeting—The *hrs* knock-out mice have an embryonic lethal phenotype, as described previously (26, 31). To analyze the biological significance of Hrs *in vivo*, we sought to generate conditional *hrs* gene-targeted mice. The targeting construct was designed to delete exon 6 of the *hrs* genomic sequence (Fig. 1*A*). Exon 6 (*E6*) codes for amino acids 139–156, and therefore, the resultant *hrs* gene-targeted allele was expected to code for an Hrs protein with a minimal N-terminal portion that lacked part of the VHS domain (amino acids 1–138). After a positive-negative selection screen, several recombinant ES clones were selected and injected into blastocysts. The chimeric mice obtained were crossed with each other to obtain heterozygous mice ($hrs^{+/floxP}$). The genotype was confirmed both by Southern blot and genomic PCR analyses (Fig. 1, *B* and *C*). Although the heterozygous mice were viable and fertile, when they were intercrossed we did not obtain viable $hrs^{floxP/floxP}$ offspring. Indeed, our timed breeding experiments revealed that the $hrs^{floxP/floxP}$ embryos were not viable after E10.5 (data not shown). We concluded that the conditional hrs^{floxP} allele was nonfunctional. Although we were unable to establish cell lines from our original *hrs* gene knock-out mice (26) because the allele still produced a C-terminal-truncated Hrs (amino acids 1–454), these new mutant $hrs^{floxP/floxP}$ embryos were ideal for preparing mouse embryonic fibroblastoid cells (MEFs). We successfully prepared MEFs from E9.5 embryos, and among randomly prepared MEF cells only the $hrs^{floxP/floxP}$ MEFs failed to survive after a few passages; in comparison, wild-type MEFs survived for many passages. We immortalized the $hrs^{+/+}$ and $hrs^{floxP/floxP}$ MEFs using the SV40 large T antigen. We obtained an immortalized cell line carrying the $hrs^{floxP/floxP}$ genotype and a control $hrs^{+/+}$ cell line, MEFw. Next, the *hrs* gene and the neomycin resistance gene (*neo*^{r}) were fully inactivated by deleting the gene segment encoding exon 6. By introducing the transient expression of Cre recombinase into the cells carrying the $hrs^{floxP/floxP}$ genotype, we obtained a cell line, HRSd, with the $hrs^{\delta/\delta}$ genotype. Deletion of the region flanked by the two loxP sequences was confirmed by genomic PCR (Fig. 1*D*). Although the δ allele could potentially have produced an N-terminal 138-amino acid fragment, the defective expression of

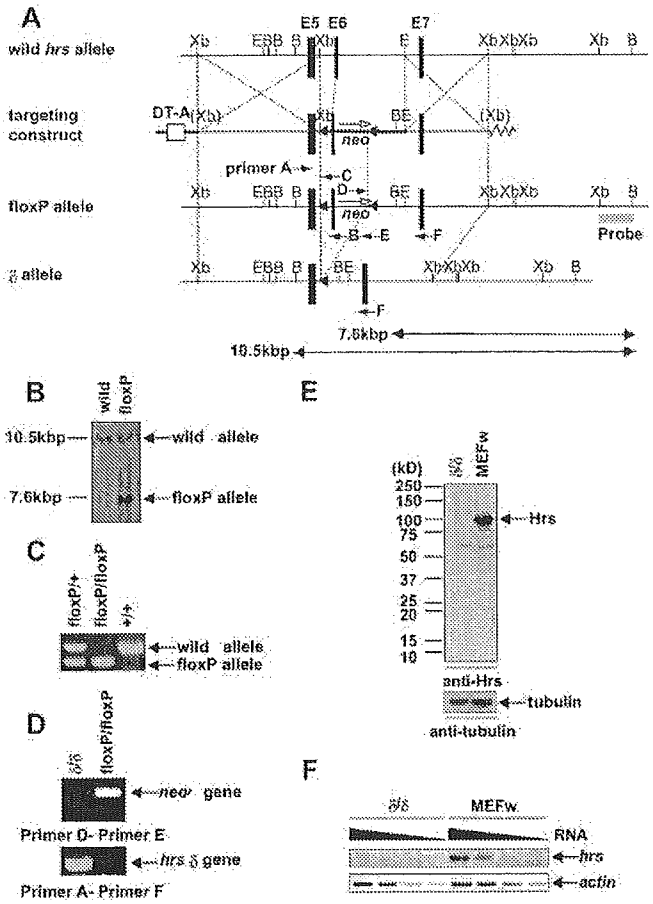

FIG. 1. **Targeted disruption of the *hrs* gene.** *A*, schematic restriction maps of the wild-type, targeting construct, and mutant alleles. The mutated allele is shown in its floxP and δ forms. *E5*, *E6*, and *E7* stand for exons 5, 6, and 7 of the *hrs* genome. *B*, *Xb*, and *E* stand for the restriction sites for BamHI, XbaI, and EcoRI, respectively. The 3′ probe used for the analytical Southern blot is shown. Primer pairs used to detect the targeted allele are shown; primers A and C for the first loxP-containing joint region and primers D and E for the neomycin-resistance gene (*neo*^{r}). *B*, a representative genomic Southern blot analysis for the wild-type (*wild*) and recombinant (*floxP*) alleles from ES cells. Genomic DNAs extracted from ES cell clones were digested with BamHI. After gel separation and blotting, the filter was hybridized with the 3′ probe. The 10.5- and 7.6-kilobase pair (*kbp*) fragments indicate wild-type and recombinant alleles, respectively. *C*, PCR-genotyping analysis of *hrs* in embryonic cell lines derived from wild-type (+/+), heterozygous (floxP/+), and homozygous (floxP/floxP) embryos. The lengths of the PCR fragments are 330 and 160 bp for the wild-type and mutant alleles, respectively. *D*, Cre-mediated deletion of *neo*^{r}. An immortalized fibroblastoid cell line with the floxP/floxP genotype was treated with Cre, and PCR analyses of the *neo*^{r} and *hrs* δ gene were performed. *E*, immunoblot analyses of the Hrs protein in an immortalized knock-out (δ/δ) and a control cell line (MEFw). *F*, semiquantitative RT-PCR analyses of the *hrs* and *β-actin* expression in HRSd and MEFw cells. Templates were prepared to make a series of 3-fold dilutions.

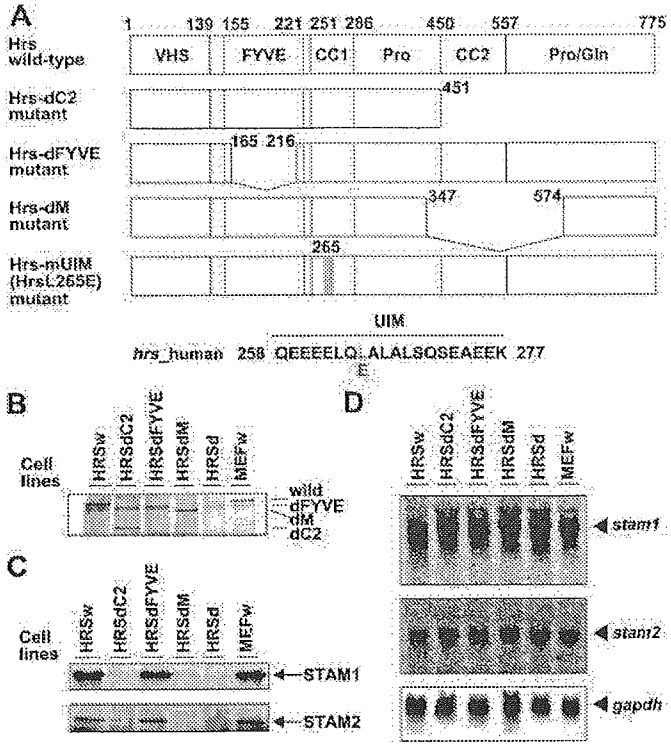

FIG. 2. **Decreased STAM1 and STAM2 in HRSd and in the presence of Hrs mutants lacking the ability to associate with the STAMs.** *A*, structures of wild-type Hrs and four mutants: *VHS*, *FYVE*, coiled-coil (*CC1* and *CC2*), proline-rich (*Pro*), and proline/glutamine-rich (*Pro/Gln*) domains. Hrs-dC2 lacks the C-terminal 326 amino acid residues, Hrs-dFYVE lacks the FYVE domain, and Hrs-dM lacks the region spanning $Pro^{348}$and Met^{573}. Hrs-mUIM (HrsL265E) carries a leucine (*L* in *red*) to glutamic acid (*E* in *blue*) point mutation at amino acid 265. *B*, the Hrs-deficient cell line (HRSd) and its sublines stably expressing wild-type Hrs, Hrs-dC2, Hrs-dFYVE, and Hrs-dM, respectively, were examined for the expression of Hrs proteins. The MEFw cell line was the control. Rabbit anti-Hrs antibody was used to detect the Hrs proteins. *C*, protein levels of STAM1 (*upper panel*) and STAM2 (*lower panel*). Lysates from the Hrs-deficient cell line (HRSd) and its sublines were used for immunoprecipitation and immunoblotting with an anti-STAM1 monoclonal antibody (TUS-1) and an anti-STAM2 monoclonal antibody (ST2–2), respectively. *D*, mRNA expression of STAM1 and STAM2 in HRSd and its sublines. Total RNAs were used for the detection of STAM1 (*stam1*) and STAM2 (*stam2*) mRNA. mRNA levels of the glyceraldehyde-3-phosphate dehydrogenase gene (*gapdh*) were monitored as the control.

both Hrs and the smaller protein in HRSd cells was confirmed with anti-Hrs antisera (Fig. 1*E*). We then performed RT-PCR experiments to determine if any mRNA containing the intact coding region within *hrs* could be detected. However, we could not detect any mRNA for *hrs* in HRSd cells (Fig. 1*F*). We, therefore, concluded that HRSd cells display a null phenotype. A gross microscopic analysis showed both the HRSd and MEFw cell lines displayed a similar flat cell shape (data not shown).

Stability of STAM1 and STAM2 Is Dependent on Hrs—Our previous experiments indicated that STAM1 and STAM2 bind directly to Hrs and are involved in the vacuolar membrane transport machinery (4, 32). To analyze the function of Hrs and its subdomains, we established HRSd sublines stably expressing wild-type (HRSw) or the dC2 (HRSdC2), dFYVE (HRSdFYVE), or dM (HRSdM) mutants of Hrs (Fig. 2, *A* and *B*). We first examined the level of the Hrs-associated proteins STAM1 and STAM2 in the mutant and MEFw lines. Although significant STAM1 protein was detected in the HRSw and MEFw cells, only minimal STAM1 was detected in HRSd cells (Fig. 2*C*). Interestingly, HRSdFYVE cells displayed a level of STAM1 similar to the level expressed by HRSw and MEFw cells, whereas the dC2 and dM mutants exhibited severely reduced levels of STAM1 (Fig. 2*C*). A similarly defective level of STAM2 was observed in HRSd, HRSdC2, and HRSdM cells (Fig. 2*C*). These results suggest that Hrs contributes to the levels of both STAM1 and STAM2 and that the Hrs region responsible for this contribution lies within amino acids 451–574, which includes the CC2 domain.

We next investigated the mechanism underlying the severely decreased levels of STAM1 and STAM2 in HRSd, HRSdC2, and HRSdM. To determine whether the suppression of STAM1/STAM2 was controlled at the transcriptional or post-transcriptional level, mRNAs prepared from HRSd and its sublines were subjected to Northern blotting. The results clearly indicated that there was little if any difference in the mRNA expression of STAM1 or STAM2 among these cell lines (Fig. 2*D*). Taken together, these results indicate that the decrease in STAM levels in the dC2 and dM Hrs mutants was post-transcriptional and was due to protein instability.

Degradation of STAM1 Is Regulated by the STAM Interaction Domain of Hrs—Since Hrs is involved in the vacuolar membrane transport machinery, we speculated that Hrs might contribute to the stability of the STAM1 protein. Therefore, we tested the possibility that Hrs is critical in regulating STAM1 degradation. To examine this possibility, HRSd cells were transiently transfected with expression vectors encoding epitope-tagged STAM1 (STAM1-V5) and Hrs. We monitored STAM1 degradation in the presence of cycloheximide (to stop *de novo* protein synthesis) by Western blotting. Although the initial level of STAM1 decreased significantly in the presence of Hrs, the degradation rate accelerated significantly in its absence (Fig. 3*A*). A similar accelerated degradation in the absence of Hrs was detected when STAM2 was tested (data not shown).

To further clarify the rate of STAM1 degradation, we performed a pulse-chase analysis of STAM1 protein expression in the presence or absence of Hrs. Hrs-deficient HRSd cells were co-transfected with a STAM1 expression plasmid along with wild-type Hrs or control vectors, and the cells were then metabolically radiolabeled. A similar level of radiolabeled STAM1 protein was detected in the presence or absence of Hrs just after the labeling period (time 0), suggesting comparable protein synthesis for STAM1 irrespective of Hrs (Fig. 3*B*). In the presence of Hrs, the radiolabeled STAM1 was slightly increased at the initial 2-h time point after the chase, probably reflecting the ongoing *de novo* protein synthesis from the incorporated amino acid pool, as previously reported (33, 34). At 8 h after the chase, STAM1 protein decreased to 30% of the initial level; in contrast, in the presence of Hrs, 80% of the initial amount of STAM1 was observed. We also investigated the effect of various Hrs subdomains on the stability of STAM1. After transient transfection with the STAM1 and Hrs expression constructs, irrespective of whether wild-type or mutant Hrs was used, ~50% of the cells co-expressed STAM1 and Hrs, with a negligible portion expressing only STAM1 (data not shown). Based on this observation, we concluded that this assay was useful for monitoring the effect of Hrs on STAM1 instability. In the absence of Hrs, a relatively fast decrease of STAM1 to 40% of its initial level was observed 6 h after the chase, which was similar to its rate of decrease in the presence of the Hrs-dM mutant (Fig. 3*C*). Consistent with our previous experiment, wild-type Hrs resulted in 80% of the radiolabeled STAM1 remaining after the chase. To determine if the UIM domain of Hrs was involved in the degradation of STAM1, we introduced a point mutation into Hrs, in which the leucine residue at amino acid position 265 was replaced by glutamic acid, resulting in this failure of the construct to bind ubiquitin (*Hrs-mUIM*, Fig. 2*A*). However, the degradation rate in the

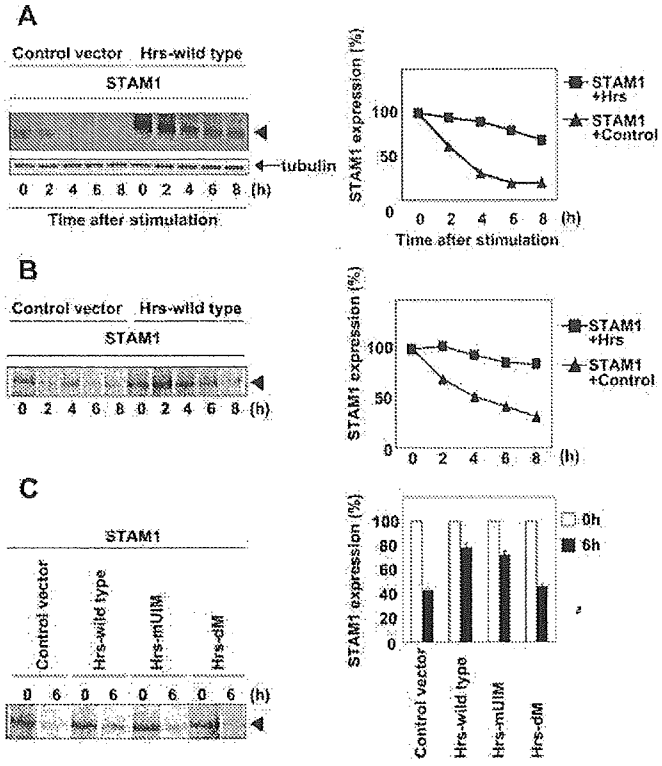

FIG. 3. **Degradation of STAM1 is controlled by Hrs.** *A*, HRSd cells were transfected with the V5-tagged STAM1 expression vector together with Hrs or a control vector. After 48 h in culture, the cells were serum-starved for 1 h and then incubated with 25 μg/ml cycloheximide. The cell lysates were immunoblotted. STAM1-V5 (*arrowhead*) and α-tubulin (tubulin) are indicated. The signal density was analyzed with a FluoroImager, and the relative densities to the initial STAM1 expression level were determined. *B*, HRSd cells were transfected with a V5-tagged STAM1-expression vector and the Hrs or control vectors. After 48 h in culture, the cells were radiolabeled with 100 μCi/ml [^{35}S]methionine/cysteine for 30 min at 37 °C and further cultured for the indicated times. After extensive washes, the STAM1 protein was recovered by immunoprecipitation with the anti-V5 antibody and monitored for radioactivity. Signals from the V5-tagged STAM1 are indicated by *arrowheads*. The amounts of radioactivity were determined. *C*, effect of wild-type Hrs and Hrs mutants on the degradation of STAM1 in HRSd cells. HRSd cells were transfected with STAM1-V5 or the control vector and radiolabeled as described in *B*. Signals from V5-tagged STAM1 are indicated by *arrowheads*. Radioactivity from STAM1 at the 0- and 6-h time points was measured, and the relative protein amount detected by the Imager is shown.

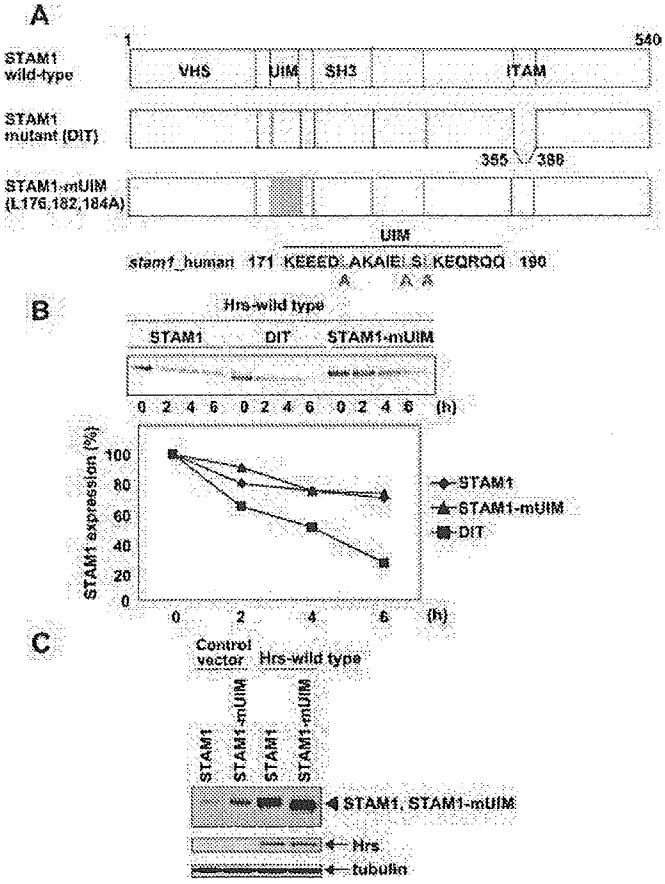

FIG. 4. **Effect of Hrs on the degradation of STAM1 and its mutants in 293T cells.** *A*, schematic structures of wild-type STAM1 and its mutants, DIT, and STAM1-mUIM. *SH3*, Src homology domain. The DIT mutant lacks the ITAM. STAM1-mUIM carries three point mutations in leucines at positions 176, 182, 184, which are replaced by alanines (leucines, *L* in *red*, replaced by alanines, *A* in *blue*). *B*, 293T cells were transfected with Hrs and STAM1-V5, DIT-V5, or STAM1-mUIM-V5. After 48 h in culture, the cells were labeled with 100 μCi/ml [^{35}S]methionine/cysteine for 30 min at 37 °C and chased for the indicated times. The STAM1-V5, DIT-V5, or STAM1-mUIM-V5 was immunoprecipitated with the anti-V5 antibody. The total amount of radioactivity in each lane was determined. *C*, Hrs-deficient cells (HRSd) were transfected with STAM1-V5 or STAM1-mUIM-V5 in combination with control or wild-type Hrs vectors. Lysates were subjected to immunoblotting with anti-V5, anti-Hrs, and anti-tubulin antibodies.

presence of Hrs-mUIM was similar to the result with wild-type Hrs (Fig. 3*C*). These results indicate that Hrs contributes to the protein stability of STAM1, for which the STAM1-association domain of Hrs is required, but the UIM domain of Hrs is not.

STAM1 Stability Is Mediated via Hrs Binding, and the UIM Domain of STAM1 Is Required for Its Stabilization—We next examined which STAM1 subdomains were responsible for the Hrs-mediated stabilization of STAM1. For this study, we used two V5-tagged STAM1 mutants, STAM1-DIT and STAM1-mUIM. STAM1-DIT lacked ITAM, an Hrs binding domain (16), and STAM1-mUIM carried three amino acid substitutions from Leu to Ala at amino acids 176, 182, and 184 in the UIM domain; these substitutions abrogated its ubiquitin binding ability (Fig. 4*A*). 293T cells were transiently co-transfected with wild-type Hrs along with wild-type STAM1 or its mutants. Whereas the level of metabolically radio-labeled STAM1-DIT gradually decreased to about 25% of its initial level during a 6-h chase, wild-type STAM1 and STAM1-mUIM showed less degradation, decreasing only to 80% by 4 h after the chase and then gradually to 70% by 6 h (Fig. 4*B*). Since the DIT mutant could not bind wild-type Hrs, these results suggest that a direct interaction between Hrs and STAM1 is required for the stability of STAM1.

To further examine the effect of Hrs on the degradation/stability of STAM1, we used the HRSd cells. Compared with wild-type STAM1, the amount of STAM1-mUIM was significantly greater, even in the absence of Hrs (Fig. 4*C*). In addition, the expression levels of both STAM1 and STAM1-mUIM were much higher in the presence of Hrs than in its absence (Fig. 4*C*). These results suggest that the UIM domain of STAM1 is essential for the stability of STAM1, and the co-expression of Hrs significantly augments the STAM1 protein stability.

STAM1 Is a Polyubiquitinated Protein and Is Degraded in a UIM-dependent Manner by Proteasomes—Our results to this point indicated that STAM1 could be degraded by either of the two main protein degradation pathways, *i.e.* the lysosomal or ubiquitin-proteasomal pathways (35). To define the degradation pathway of STAM1, we first examined the effects of lactacystin, a potent and selective proteasome inhibitor, and of a lysosome inhibitor, E-64-d, on the stability of STAM1 in the absence of Hrs. HRSd cells were transiently co-transfected with wild-type STAM1 and HA-tagged ubiquitin in the presence or absence of lactacystin. Incubation with lactacystin in-

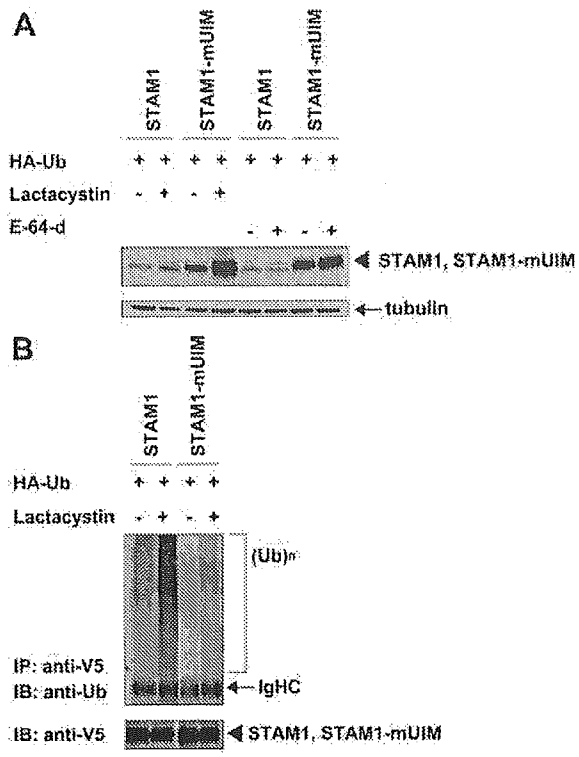

FIG. 5. **STAM1 was degraded by the ubiquitin-proteasome pathway via its UIM.** *A*, HRSd cells were transfected with STAM1-V5 or STAM1-mUIM-V5 in combination with HA-tagged ubiquitin and then cultured with H_2O, 10 μM lactacystin, or 100 μM E-64-d for 10 h. Cells were lysed in 1% Nonidet P-40 cell lysis buffer, and the lysates were used for immunoprecipitation and immunoblotting with the anti-V5 antibody. *B*, immunoprecipitation (*IP*) analysis of STAM1 proteins from 293T cells. 293T cells were transfected with STAM1-V5 or STAM1-mUIM-V5 in combination with HA-tagged ubiquitin and then cultured with H_2O or 10 μM lactacystin for 10 h. Cell lysates were used for immunoprecipitation with the anti-V5 antibody and immunoblotted (*IB*) with the anti-ubiquitin or anti-V5 antibody.

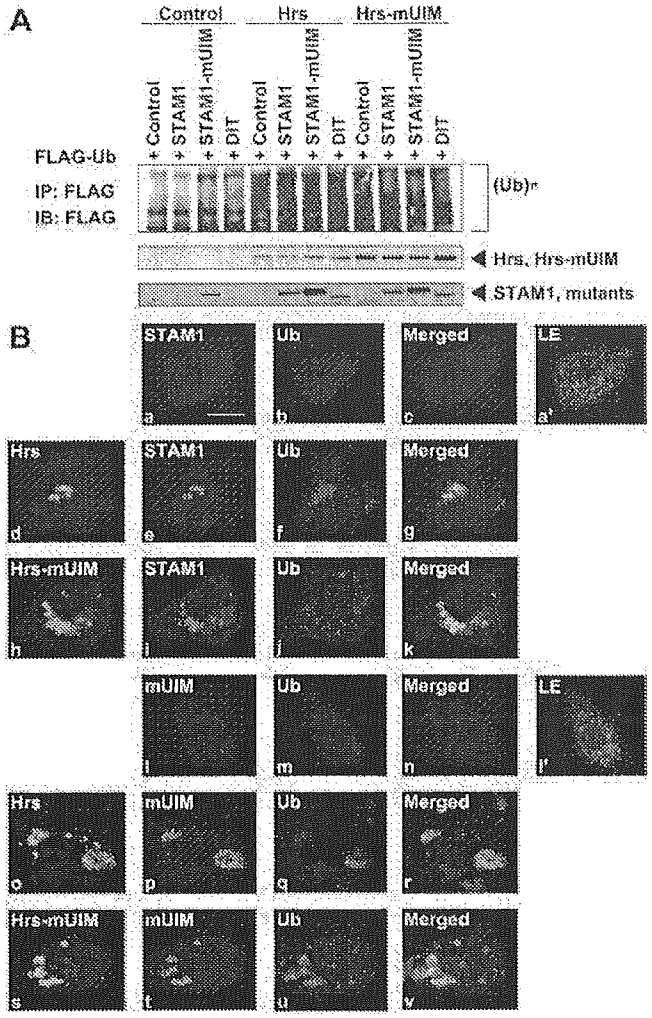

FIG. 6. **Overexpressed Hrs accumulated as a ubiquitinated protein.** *A*, HRSd cells were transfected with the control vector, STAM1-V5, or its mutants in the presence or absence of wild-type Hrs or Hrs-mUIM in combination with FLAG-tagged ubiquitin. Lysates of these cells were used for immunoprecipitation (*IP*) and immunoblotting (*IB*) with the anti-FLAG antibody. Cell lysates were immunoblotted with rabbit anti-Hrs and anti-V5 antibodies. *B*, wild-type Hrs, Hrs-mUIM, STAM1-V5, STAM1-mUIM-V5, and ubiquitin in the early endosome. HRSd cells were transiently transfected with the indicated plasmids. The cells were double- or triple-labeled with the indicated antibodies and fluorescence-conjugated secondary antibodies: Hrs (Alexa 488 (*green*)), STAM1 (Alexa 594 (*red*)), and ubiquitin (Alexa 350 (*blue*)) are shown. Images taken with a longer exposure (*LE*) for *a* and *l* are shown in *a'* and *l'*. *Bars* indicate 20 μm.

creased the amount of wild-type STAM1 protein (Fig. 5*A*). Interestingly, STAM1-mUIM was significantly more stable than wild-type STAM1 even in the absence of lactacystin, and its stability increased profoundly in the presence of lactacystin. On the other hand, E-64-d showed little if any effect on STAM1 stability.

Since protein degradation by proteasomes is regulated by protein ubiquitination, we asked whether STAM1 was ubiquitinated. 293T cells were transiently co-transfected with wild-type STAM1 and HA-tagged ubiquitin. The co-transfected cells were subjected to immunoprecipitation with the anti-V5 antibody, and the ubiquitins in the precipitates were analyzed (Fig. 5*B*). Although the V5 tag contains one lysine residue, our preliminary experiments suggested that this lysine receives little if any modification by ubiquitin (data not shown). As expected, ubiquitin clearly co-precipitated with STAM1. Furthermore, the prior treatment of cells with lactacystin significantly increased the degree of ubiquitination. The protein expression levels of wild-type STAM1 and STAM1-mUIM did not differ significantly in our hands, probably because of the expression of endogenous Hrs in the 293T cells. Collectively, these results suggest that STAM1 is a polyubiquitinated protein, and mutations of its UIM domain severely abolish the ubiquitination.

STAM1·Hrs Complex Is Responsible for Ubiquitin Accumulation on/within the Endosomes—To clarify whether the STAMs and Hrs contribute to the accumulation of cellular ubiquitinated proteins, we co-transfected HRSd cells with the STAM1 and Hrs expression vectors and FLAG-tagged ubiquitin. Whole-cell lysates were then tested for the intracellular accumulation of ubiquitinated proteins. In the absence of Hrs, the introduction of wild-type STAM1 and DIT resulted in little if any increase in the amount of ubiquitin accumulation (Fig. 6*A*). Transfection of STAM1-mUIM slightly increased the ubiquitination. However, the introduction of Hrs caused a marked accumulation of ubiquitinated proteins irrespective of the presence of STAM1. Unexpectedly, a slightly smaller amount of ubiquitins accumulated in the presence of Hrs-mUIM than in the presence of wild-type Hrs even though Hrs-mUIM seemed more stable than wild-type Hrs (Fig. 6*A*, *middle panel*). These results indicate that Hrs is responsible for the intracellular accumulation of ubiquitinated proteins, independent of STAM1.

We next asked whether the presence of STAM1 and Hrs could affect the endosomal localization and accumulation of ubiquitinated proteins. Consistent with our earlier results,

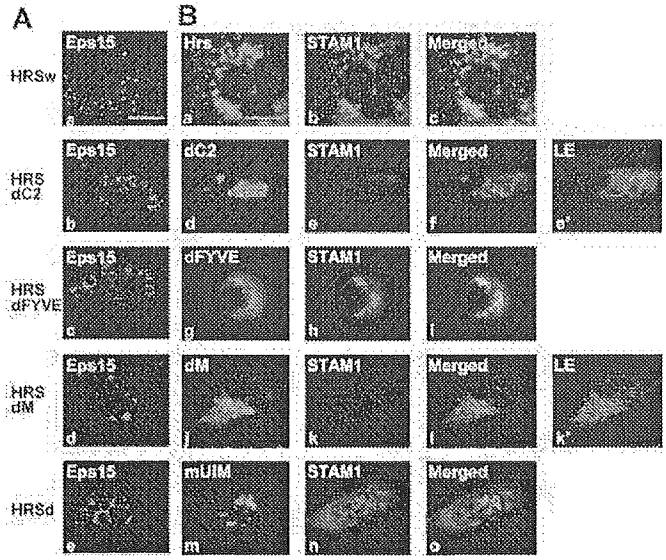

FIG. 7. **UIM mutant of Hrs confers endosome enlargement phenotype.** *A*, early endosome phenotypes detected by Eps15 expression. HRSd and its sublines were transiently transfected with the Eps15 expression vector. Eps15 is shown in *red*. *Bars* indicate 20 μm. *B*, localization of wild-type Hrs, its mutants, and STAM1. HRSd cells were transiently transfected with various Hrs expression vectors and STAM1 expression plasmids. Hrs is shown in *green* (Alexa 488), and STAM1 is shown in *red* (Alexa 594). Images taken with a longer exposure (*LE*) for *e* and *k* are shown in *e'* and *k'*. *Bars* indicate 20 μm.

when HRSd cells were transfected with STAM1 and ubiquitin, only faint STAM1 labeling was observed (Fig. 6*B*, *a*). In contrast, the co-introduction of wild-type Hrs and STAM1 resulted in the colocalization of these proteins (Fig. 6*B*, *d*, *e*, and *g*). Interestingly, heavy staining of ubiquitinated proteins overlapped with the staining of the STAM1·Hrs complex (Fig. 6*B*, *f* and *g*). Surprisingly, the introduction of Hrs-mUIM and STAM1 into HRSd cells induced enlarged endosomes in which the Hrs-mUIM and STAM1 immunoreactivity overlapped that of the ubiquitins (Fig. 6*B*, *h–k*).

Next, we examined whether the UIM of STAM1 played a role in the endosomal localization of these proteins and/or the endosomal phenotypes. When HRSd cells were transfected with STAM1-mUIM and ubiquitin, a slightly but significantly stronger signal for the STAM1-mUIM than for wild-type STAM1 was detected in the cytoplasm with a marginal increase in cytoplasmic ubiquitin expression (Fig. 6*B*, *l–l'*). In the presence of wild-type Hrs, the expression of STAM1-mUIM resulted in almost normal-sized endosomes that were co-localized with ubiquitins (Fig. 6*B*, *o–r*). However, when both STAM1 and Hrs were mutated at their UIM domains the HRSd cells clearly showed enlarged vesicles that co-localized with ubiquitins (Fig. 6*B*, *s–v*). These results suggest that Hrs and STAM1 co-localized with ubiquitinated proteins, and the intact UIM domain of Hrs but not of STAM1 is required for normal endosomal development. Collectively, these results suggest that Hrs is indispensable for the intracellular accumulation and endosomal localization of ubiquitins.

The UIM Domain of Hrs Is Essential for Enlarged Endosome Formation—Enlarged endosomes in the absence of Hrs have been reported (31, 32). We also examined the phenotypes of early endosomes in HRSd sublines expressing wild-type Hrs or its mutants using the co-expression of an endosomal marker protein, Eps15. By fluorescence microscopy, a scattered dot-like expression pattern of Eps15 was observed within the cytoplasm of HRSw cells that corresponded to the normal early endosome size and structure (Fig. 7*A*, *a*). In contrast, HRSd cells contained enlarged endosomes (Fig. 7*A*, *e*), and the two Hrs mutant cell lines Hrs-dC2 and -dFYVE exhibited a significantly enlarged endosome phenotype; the endosomes in these mutants were, however, smaller than those observed in HRSd cells (Fig. 7*A*, *b* and *c*). Cells expressing the Hrs mutant HRSdM, which fails to interact with either STAM1 or STAM2, also manifested modestly enlarged endosomes that lacked central transparency (Fig. 7*A*, *d*). Unexpectedly, the transient introduction of the Hrs-mUIM mutant also conferred an enlarged endosome phenotype (Fig. 7*B*, *m*). Thus, enlarged endosomes were observed in the absence of Hrs and in the presence of the Hrs-dC2, -dFYVE, -dM, and -mUIM mutants.

We next asked whether the subcellular localization of STAMs was altered in the presence or absence of wild-type or mutant Hrs. To examine the localization of Hrs and STAM1, we introduced Hrs and its mutants along with the STAM1 expression vector into HRSd cells (Fig. 7*B*). Consistent with the data in Fig. 7*A*, spot-like cytoplasmic expression of the wild-type Hrs and STAM1 was observed with nearly complete co-localization (Fig. 7*B*, *a–c*). Similar results were obtained when the STAM2 expression vector was introduced into HRSd cells (data not shown). Strikingly, when the Hrs-dC2 and -dM mutants were introduced, the STAM1 and Hrs mutants localized independently; Hrs localized to the enlarged endosomes, whereas STAM1 was diffusely expressed throughout the cytoplasm (Fig. 7*B*, *d–f* and *j–l*). The STAM1 immunoreactivity was significantly reduced when STAM1 was co-introduced with the Hrs-dC2 and Hrs-dM mutants but not with wild-type Hrs (Fig. 7*B*, *e* and *k*). Only long exposure images clearly showed the localization of STAM1 in the cytoplasm in the presence of these mutants (Fig. 7*B*, *e'* and *k'*). Interestingly, the Hrs-dFYVE mutant completely colocalized with STAM1, although the endosomes were enlarged and differed significantly from those seen with wild-type Hrs (Fig. 7*B*, *g–i*). These results indicate that the endosomal localization of STAM1 was dependent on its ability to bind Hrs because when it was cotransfected with Hrs mutants lacking STAM1 binding capability (HRSdC2 and HRSdM), STAM1 was expressed diffusely in the cytoplasm.

DISCUSSION

Stability of STAMs Is Dependent on Hrs—In this study we established an Hrs-deficient cell line and demonstrated the critical involvement of Hrs in the stability of both the STAM1 and STAM2 proteins. Whereas the Hrs-deficient HRSd cells showed a profound decrease in the level of STAM1 and STAM2, the stable introduction of Hrs fully restored both proteins to levels similar to those in normal MEFw cells. The drastic reduction in STAM1 and STAM2 could have been due to several possible factors, which are decreased transcription or translation, the stability of the mRNAs, or decreased protein stability. Our Northern blot analyses clearly demonstrated that the amount of STAM1 and STAM2 mRNA remained unchanged irrespective of the presence or absence of Hrs, indicating that instability of the STAM proteins accounted for the reduced levels. Similarly, transient transfection of the HRSd cells showed that the stability of both STAM1 and STAM2 was impaired. We, therefore, conclude that Hrs deficiency is likely to cause the STAM1 and STAM2 proteins to be unstable, and both proteins are therefore rapidly degraded so as to be undetectable on our regular Western blots.

Previous work by us indicated that both STAM1 and STAM2 firmly associate with Hrs through the CC2 domain of Hrs and the ITAM motif of STAM1 and STAM2 (4). Hrs probably binds the STAMs at a ratio of one to one, given that we observed only STAM1-Hrs and STAM2-Hrs heterodimeric complexes, but not a STAM1, STAM2, and Hrs trimeric complex (32). Here, neither STAM1 nor STAM2 was detected in HRSdC2 or HRSdM

cells, suggesting that the region containing the CC2 domain (amino acid 348–573) is necessary for the stability of the STAMs. Since the STAM proteins were detected in the Hrs-dFYVE mutant cell line, the FYVE domain of Hrs, which is required for Hrs to bind the inner surface of the cytoplasmic membrane through phosphatidylinositol 3,4,5-trisphosphate, is not necessary for the stability of the STAMs. The expression levels of Hrs in the Hrs-dC2 and Hrs-dM mutant cell lines, however, were markedly reduced and accompanied by the loss of STAM1 and STAM2. These results suggest that Hrs stabilizes the STAMs by directly binding to them.

The ITAM domain of STAM1 and STAM2 is required for binding to Hrs, although an additional region, called the SSM domain (in human STAM1, amino acids 297–320 and human STAM2 amino acids 286–309) may possess auxiliary Hrs binding functions (36). Given that the Hrs-dC2 mutation resulted in the degradation of STAM1, we expected the STAM1-DIT mutant, which is incapable of binding to Hrs, to be unstable. Consistent with this, the degradation of the STAM1-DIT mutant was significantly faster than that of wild-type STAM1. Our previous report using STAM1/STAM2 double-deficient cells clearly demonstrated that Hrs protein degradation is not controlled by the STAMs (32). Furthermore, a recent report showed that an Hrs knockdown induces Tsg101 instability, suggesting that Hrs also helps stabilize Tsg101. Since Tsg101 was recently shown to interact with Hrs and is now categorized as an ESCRT-I molecule, Hrs may function to stabilize other proteins as well (37). Taken together, our results show that STAM1 is stabilized by an association with Hrs, and Hrs mutants that disrupt STAM1 binding result in STAM1 degradation.

How does the deficiency of Hrs mediate STAM1 and STAM2 protein stability? In general, there are two major protein degradation systems, the ubiquitin-proteasome and the lysosome/vacuole pathways. These two pathways seem to regulate protein fate differentially, so that proteins with short half-lives tend to be degraded by the ubiquitin-proteasome pathway, whereas those with long half-lives are more likely to be digested by the lysosome/vacuole pathway (35). Our present results clearly indicated that the STAM1 degradation was proteasome-dependent. This was unexpected, because both STAMs and Hrs were previously shown to be resident endosomal proteins and believed to function in the endosome maturation machinery. A possible scenario, taken from recent data, is that the ESCRT complex could mediate protein degradation through a vesicular transport function (1). In this hypothesis protein ubiquitination has an indispensable function for transport. According to our present data, as long as Hrs is present ubiquitinated proteins can accumulate within the endosomes. Since the STAMs can hardly be detected in the absence of Hrs, we cannot fully exclude the possibility that STAM1 plays a role in the accumulation of ubiquitinated proteins within endosomes. Nevertheless, our data provide further evidence supporting the idea that ESCRT proteins mediate the accumulation of ubiquitinated proteins into endosomes, where the proteins are destined to be degraded in a lysosome-dependent manner.

Both the STAMs and Hrs possess a UIM domain, which was first identified as a polyubiquitin-binding site in the S5a subunit of the 26 S proteasome (38). The results of our mutational analysis suggest that the UIM domain of Hrs is not involved in the degradation of STAM1. However, the UIM domain of STAM1 is essential for its stability. A STAM1 mutant with point mutations within the UIM (STAM1-mUIM) was significantly more stable than wild-type STAM1 (STAM1-UIM), indicating that STAM1 controls its own degradation by the proteasome pathway. At present we have at least three hypotheses to explain the STAM1-UIM function. First, the UIM of STAM1 may contain one or more major polyubiquitinated sites. The UIM domain of STAM1 contains three lysine residues (Lys-171, Lys-178, and Lys-185) that are potentially polyubiquitinated and destined to be recognized by the 26 S proteasome for degradation. Indeed, of the three lysine residues, the first two are evolutionarily conserved from *Drosophila* to human. Although lysine 171 is a potential protein modification site for both ubiquitination and sumoylation, it is unlikely to play an important role in this degradation, since our UIM mutant conserves all three lysine residues (39). Second, the UIM domain of STAM1 may interact with other polyubiquitinated proteins, which will be recognized and degraded by the proteasome. However, it is unknown whether the degradation of any given protein can be mediated via interactions with another ubiquitinated protein(s). Recently, Hrs was shown to interact with AIP4, a HECT domain-containing E3 ubiquitin ligase (40). We, therefore, propose a third mechanism whereby the UIM domain of STAM1 interacts with an E3 enzyme(s) either alone or as a complex and, thus, allows STAMs to be ubiquitinated and thereby destined for degradation. Hrs is ubiquitinated by AIP4 and mediates the sorting of chemokine receptor CXCR4 into endosomes (40). In agreement with this, we also detected a significant increase in the level of the Hrs-mUIM protein compared with wild-type Hrs, suggesting its stabilization through the UIM via interactions with one or more ubiquitinase enzymes. We provide direct evidence that the UIM domain of Hrs (or some other UIM-interaction protein(s)) is not required for STAM1 degradation. To further analyze the mechanism underlying the degradation of STAMs, it will be necessary to identify an E3 enzyme that couples with the STAMs.

Hrs Causes Accumulation of Ubiquitinated Proteins—Previous studies have shown that the UIM domains of mammalian Hrs and yeast Vps27 are both essential for sorting ubiquitinated membrane proteins into the degradation pathway (2, 12, 41). Consistent with this, Hrs binds to monoubiquitinated proteins through its UIM domain (2, 12, 41). However, little is known about the role Hrs plays in intracellular polyubiquitination. The introduction of Hrs into HRSd cells caused the marked elevation of ubiquitinated proteins irrespective of the presence of STAM1 expression vectors. At present, the mechanism underlying the ubiquitinated protein accumulation is unclear. It is clear that the aberrantly enlarged endosomes do not account for the ubiquitin accumulation within whole-cell extracts because the class E compartment does not show any accumulation of ubiquitinated proteins in the absence of Hrs but, rather, manifests a significant decrease in ubiquitinated proteins. One possible explanation is that Hrs may control the activity of an E3 ubiquitin ligase. Cargo proteins captured by Hrs could be stabilized and/or further receive ubiquitination, probably through E3 group ubiquitinases within the Hrs complex. However, since the Hrs-mUIM mutant showed only a marginal decrease in intracellular ubiquitination, it may be that other E3 ligases are involved in ubiquitin accumulation. Since STAM1, STAM2, and Tsg101, which all belong to the ESCRT complex, possess additional ubiquitin-binding motifs, ESCRT molecules including Hrs may function as a complex to increase protein ubiquitination and/or protein stabilization. Conversely, our present data suggest that at least some ubiquitinated proteins accumulate within the endosomes. Therefore, ubiquitinated proteins destined to be degraded by the late endosome/lysosome system may be modified by Hrs. Interestingly, the overexpression of STAM2 in the presence of Hrs was recently reported to significantly increase the levels of intracellular ubiquitinated

proteins (36, 42). Our present data using Hrs-defective cells clearly indicate that the overexpression of STAM1 does not lead to an increase in ubiquitinated proteins. This difference might be due to the effects of excessive amounts of STAM2 and/or the presence of native Hrs in their experiment. Although further experiments are needed to clarify the mechanism, we propose that dysregulation of the STAM·Hrs complex may affect intracellular ubiquitination accumulation and the degradation machinery.

Enlarged Endosome Phenotype Is Dependent on Hrs—Recent studies by us (32) and others (19, 42) have provided evidence that the STAMs and Hrs co-localize in early endosomes. An earlier report demonstrated that Hrs can be co-immunoprecipitated with Eps15, an endosomal marker protein (43). Hrs has also been shown to bind Eps15 through the N-terminal half of Hrs (44). The direct binding of STAM1 with Eps15 was also reported (43). Since Eps15, an early endosomal membrane protein, is involved in the endocytosis of membrane-associated receptors via its binding to AP-2 (45), both the STAMs and Hrs are also localized to the same vesicles.

The lack of Hrs triggers aberrant intracellular vesicle formation called class E compartments. This was first demonstrated in genetic analyses with yeast mutants manifesting similar large vesicular compartments (2). In this report, we also clearly demonstrated abnormally enlarged endosomes. This "mammalian class E compartment" was present in several Hrs mutants we tested that were introduced into HRSd cells. Although the degree of endosomal enlargement differed with the mutation, our present data suggest that the class E phenotype is dependent on the C-terminal, FYVE, or CC2 domain. We therefore speculate that intact Hrs is required for endosomes to have a normal appearance. Interestingly, a point mutation (L265E) within the UIM domain of Hrs abrogates the normal endosomal architecture. It is possible that an unidentified UIM interaction molecule(s) functions in the normal endosomal phenotype. Unlike the UIM of Hrs, point mutations within the UIM of STAM1 did not result in enlarged endosomes. The class E compartment phenotype can be determined, therefore, by the UIM domain of Hrs but not by that of the STAMs. It is of note that Hrs not only supported the protein stability of STAMs but also determined their intracellular localization; the absence of Hrs totally changed the localization of STAMs from the endosomes to the cytoplasm. On the other hand, Hrs, whether wild type or mutated, always localized to the endosomes. To understand how this co-localization occurs, further work will be required to identify the region(s) within Hrs that is responsible for its localization.

In Vivo Function of Hrs—We provide further evidence that Hrs is required for normal mouse development. Although our attempt to establish a conditional targeting mouse has been unsuccessful, probably because of the impaired function of the *"floxed"* exon 6, experiments using established cell lines carrying the null allele provided the unexpected finding that the Hrs knock-out leads to the functional extinction of the STAM1 and STAM2 proteins. Incidentally, the STAM1/STAM2 double-knock-out mice we have generated die *in utero* around E11.5, because the ventral fold fails to form.[2] It is not surprising that Hrs knock-out mice with no detectable STAM1 or STAM2 protein manifest an embryonic lethal phenotype as well (26, 31). Loss of Hrs and/or STAM function results in mammalian class E phenotypes, which are similar to the class E phenotypes of yeast Vps27 and Hse1. Paradoxically, an excess of Hrs protein seems to be toxic to cells, because the overexpression of Hrs leads to a similar enlargement of endosomes (13). These results suggest that the appropriate control of Hrs and STAM1/STAM2 may be critical for normal cell morphology and function. Given that Hrs is involved in the accumulation of intracellular ubiquitinated proteins, our next step should be to clarify the functional relationship between the ESCRT complex and the ubiquitination machinery.

[2] H. Kobayashi, N. Tanaka, S. Miura, and K. Sugamura, unpublished data.

REFERENCES

1. Raiborg, C., Rusten, T. E., and Stenmark, H. (2003) *Curr. Opin. Cell Biol.* **15,** 446–455
2. Bilodeau, P. S., Urbanowski, J. L., Winistorfer, S. C., and Piper, R. C. (2002) *Nat. Cell Biol.* **4,** 534–539
3. Takeshita, T., Arita, T., Asao, H., Tanaka, N., Higuchi, M., Kuroda, H., Kaneko, K., Munakata, H., Endo, Y., Fujita, T., and Sugamura, K. (1996) *Biochem. Biophys. Res. Commun.* **225,** 1035–1039
4. Asao, H., Sasaki, Y., Arita, T., Tanaka, N., Endo, K., Kasai, H., Takeshita, T., Endo, Y., Fujita, T., and Sugamura, K. (1997) *J. Biol. Chem.* **272,** 32785–32791
5. Endo, K., Takeshita, T., Kasai, H., Sasaki, Y., Tanaka, N., Asao, H., Kikuchi, K., Yamada, M., Chenb, M., O'Shea, J. J., and Sugamura, K. (2000) *FEBS Lett.* **477,** 55–61
6. Komada, M., and Kitamura, N. (1995) *Mol. Cell. Biol.* **15,** 6213–6221
7. Goodman, O. B., Jr., Krupnick, J. G., Gurevich, V. V., Benovic, J. L., and Keen, J. H. (1997) *J. Biol. Chem.* **272,** 15017–15022
8. Gaullier, J. M., Simonsen, A., D'Arrigo, A., Bremnes, B., Stenmark, H., and Aasland, R. (1998) *Nature* **394,** 432–433
9. Dell'Angelica, E. C., Klumperman, J., Stoorvogel, W., and Bonifacino, J. S. (1998) *Science* **280,** 431–434
10. ter Haar, E., Harrison, S. C., and Kirchhausen, T. (2000) *Proc. Natl. Acad. Sci. U. S. A.* **97,** 1096–1100
11. Raiborg, C., Bache, K. G., Mehlum, A., Stang, E., and Stenmark, H. (2001) *EMBO J.* **20,** 5008–5021
12. Raiborg, C., Bache, K. G., Gillooly, D. J., Madshus, I. H., Stang, E., and Stenmark, H. (2002) *Nat. Cell Biol.* **4,** 394–398
13. Komada, M., Masaki, R., Yamamoto, A., and Kitamura, N. (1997) *J. Biol. Chem.* **272,** 20538–20544
14. Chin, L. S., Raynor, M. C., Wei, X., Chen, H. Q., and Li, L. (2001) *J. Biol. Chem.* **276,** 7069–7078
15. Bishop, N., Horman, A., and Woodman, P. (2002) *J. Cell Biol.* **157,** 91–101
16. Takeshita, T., Arita, T., Higuchi, M., Asao, H., Endo, K., Kuroda, H., Tanaka, N., Murata, K., Ishii, N., and Sugamura, K. (1997) *Immunity* **6,** 449–457
17. Lohi, O., Poussu, A., Merilainen, J., Kellokumpu, S., Wasenius, V. M., and Lehto, V. P. (1998) *J. Biol. Chem.* **273,** 21408–21415
18. Pandey, A., Fernandez, M. M., Steen, H., Blagoev, B., Nielsen, M. M., Roche, S., Mann, M., and Lodish, H. F. (2000) *J. Biol. Chem.* **275,** 38633–38639
19. Bache, K. G., Raiborg, C., Mehlum, A., and Stenmark, H. (2003) *J. Biol. Chem.* **278,** 12513–12521
20. Nakai, S., Kawano, H., Yudate, T., Nishi, M., Kuno, J., Nagata, A., Jishage, K., Hamada, H., Fujii, H., and Kawamura, K. (1995) *Genes Dev.* **9,** 3109–3121
21. Schonemann, M. D., Ryan, A. K., McEvilly, R. J., O'Connell, S. M., Arias, C. A., Kalla, K. A., Li, P., Sawchenko, P. E., and Rosenfeld, M. G. (1995) *Genes Dev.* **9,** 3122–3135
22. Bermingham, J. R., Jr., Scherer, S. S., O'Connell, S., Arroyo, E., Kalla, K. A., Powell, F. L., and Rosenfeld, M. G. (1996) *Genes Dev.* **10,** 1751–1762
23. Imamoto, A., and Soriano, P. (1993) *Cell* **73,** 1117–1124
24. Tanaka, N., Kamanaka, M., Enslen, H., Dong, C., Wysk, M., Davis, R. J., and Flavell, R. A. (2002) *EMBO Rep.* **3,** 785–791
25. Niwa, H., Yamamura, K., and Miyazaki, J. (1991) *Gene (Amst.)* **108,** 193–199
26. Miura, S., Takeshita, T., Asao, H., Kimura, Y., Murata, K., Sasaki, Y., Hanai, J. I., Beppu, H., Tsukazaki, T., Wrana, J. L., Miyazono, K., and Sugamura, K. (2000) *Mol. Cell. Biol.* **20,** 9346–9355
27. Polo, S., Sigismund, S., Faretta, M., Guidi, M., Capua, M. R., Bossi, G., Chen, H., De Camilli, P., and Di Fiore, P. P. (2002) *Nature* **416,** 451–455
28. Ebisawa, T., Fukuchi, M., Murakami, G., Chiba, T., Tanaka, K., Imamura, T., and Miyazono, K. (2001) *J. Biol. Chem.* **276,** 12477–12480
29. Yamada, M., Takeshita, T., Miura, S., Murata, K., Kimura, Y., Ishii, N., Nose, M., Sakagami, H., Kondo, H., Tashiro, F., Miyazaki, J. I., Sasaki, H., and Sugamura, K. (2001) *Mol. Cell. Biol.* **21,** 3807–3819
30. Yamada, M., Ishii, N., Asao, H., Murata, K., Kanazawa, C., Sasaki, H., and Sugamura, K. (2002) *Mol. Cell. Biol.* **22,** 8648–8658
31. Komada, M., and Soriano, P. (1999) *Genes Dev.* **13,** 1475–1485
32. Kanazawa, C., Morita, E., Yamada, M., Ishii, N., Miura, S., Asao, H., Yoshimori, T., and Sugamura, K. (2003) *Biochem. Biophys. Res. Commun.* **309,** 848–856
33. van Kerkhof, P., Alves dos Santos, C. M., Sachse, M., Klumperman, J., Bu, G., and Strous, G. J. (2001) *Mol. Biol. Cell* **12,** 2556–2566
34. Koinuma, D., Shinozaki, M., Komuro, A., Goto, K., Saitoh, M., Hanyu, A., Ebina, M., Nukiwa, T., Miyazawa, K., Imamura, T., and Miyazono, K. (2003) *EMBO J.* **22,** 6458–6470
35. Onodera, J., and Ohsumi, Y. (2004) *J. Biol. Chem.* **279,** 16071–16076
36. Mizuno, E., Kawahata, K., Okamoto, A., Kitamura, N., and Komada, M. (2004) *J. Biochem. (Tokyo)* **135,** 385–396
37. Bache, K. G., Brech, A., Mehlum, A., and Stenmark, H. (2003) *J. Cell Biol.* **162,** 435–442
38. Young, P., Deveraux, Q., Beal, R. E., Pickart, C. M., and Rechsteiner, M. (1998) *J. Biol. Chem.* **273,** 5461–5467
39. Sampson, D. A., Wang, M., and Matunis, M. J. (2001) *J. Biol. Chem.* **276,** 21664–21669

40. Marchese, A., Raiborg, C., Santini, F., Keen, J. H., Stenmark, H., and Benovic, J. L. (2003) *Dev. Cell* **5,** 709–722
41. Shih, S. C., Katzmann, D. J., Schnell, J. D., Sutanto, M., Emr, S. D., and Hicke, L. (2002) *Nat. Cell Biol.* **4,** 389–393
42. Mizuno, E., Kawahata, K., Kato, M., Kitamura, N., and Komada, M. (2003) *Mol. Biol. Cell* **14,** 3675–3689
43. Hansen, K., Ronnstrand, L., Claesson-Welsh, L., and Heldin, C. H. (1997) *FEBS Lett.* **409,** 195–200
44. Bean, A. J., Davanger, S., Chou, M. F., Gerhardt, B., Tsujimoto, S., and Chang, Y. (2000) *J. Biol. Chem.* **275,** 15271–15278
45. van Delft, S., Schumacher, C., Hage, W., Verkleij, A. J., and van Bergen en Henegouwen, P. M. (1997) *J. Cell Biol.* **136,** 811–821

HIV-1 Vpr Induces DNA Double-Strand Breaks

Hiroaki Tachiwana,[1,2] Mari Shimura,[2] Chikako Nakai-Murakami,[2] Kenzo Tokunaga,[3] Yoshimasa Takizawa,[1,2] Tetsutaro Sata,[3] Hitoshi Kurumizaka,[1] and Yukihito Ishizaka[2]

[1]Graduate School of Science and Engineering, Waseda University; [2]Department of Intractable Diseases, International Medical Center of Japan; and [3]Department of Pathology, National Institute of Infectious Diseases, Tokyo, Japan

Abstract

Recent observations imply that HIV-1 infection induces chromosomal DNA damage responses. However, the precise molecular mechanism and biological relevance are not fully understood. Here, we report that HIV-1 infection causes double-strand breaks in chromosomal DNA. We further found that Vpr, an accessory gene product of HIV-1, is a major factor responsible for HIV-1–induced double-strand breaks. The purified Vpr protein promotes double-strand breaks when incubated with isolated nuclei, although it does not exhibit endonuclease activity *in vitro*. A carboxyl-terminally truncated Vpr mutant that is defective in DNA-binding activity is less capable of Vpr-dependent double-strand break formation in isolated nuclei. The data suggest that double-strand breaks induced by Vpr depend on its DNA-binding activity and that Vpr may recruit unknown nuclear factor(s) with positive endonuclease activity to chromosomal DNA. This is the first direct evidence that Vpr induces double-strand breaks in HIV-1–infected cells. We discuss the possible roles of Vpr-induced DNA damage in HIV-1 infection and the involvement of Vpr in further acquired immunodeficiency syndrome–related tumor development. (Cancer Res 2006; 66(2): 627-31)

Introduction

A high incidence of malignant tumors, such as non-Hodgkin's lymphoma, Kaposi's sarcoma, and invasive cervical cancer [acquired immunodeficiency syndrome (AIDS)–defining cancers], is epidemiologically associated with HIV-1 infection (1, 2). These neoplasms are attributable mainly to diseases that accompany immunodeficiency, including coinfection with EBV, human herpes virus 8, and human papillomavirus (1, 2). In addition to these AIDS-defining cancers, several non-AIDS-defining cancers also occur with a higher incidence in HIV-infected individuals (3, 4). These reports lead to the assumption that HIV-1 has the potential to induce neoplasms before AIDS develops. Recently, DNA damage responses have been observed in precancerous lesion before inactivation of p53 (5, 6). Interestingly, it has been reported that HIV-1 infection induces DNA damage responses by activating Rad3-related or ataxia-telangiectasia mutated proteins and promoting phosphorylation of their downstream substrates (7, 8). The elucidation of the factor triggering the DNA damage responses to HIV-1 infection is essential to determine the as yet unknown mechanism causing AIDS-related neoplasms. In the present study, we found that HIV-1 infection induces double-strand breaks of chromosomal DNA, as detected using pulsed-field gel electrophoresis (PFGE). We further showed that *vpr*, an accessory gene of HIV-1 encoding a virion-associated nuclear protein, which induces cell cycle accumulation at G_2-M phase and increases ploidy (9), was a factor responsible for double-strand breaks. We discuss the potential ability of Vpr-induced double-strand breaks to develop into neoplasms in HIV-1 infection.

Materials and Methods

Cell culture. MIT-23 and ΔVpr, a mock transfectant, were established from HT1080 (JCRB9113; the Health Science Research Resources Bank) as previously described (9). In MIT-23, Vpr expression is controlled by the rtet promoter on incubation with 3 μg/mL doxycycline (Sigma, St. Louis, MO) for 48 hours.

Virus infection. Vesicular stomatitis virus G protein (VSV-G)–pseudotyped HIV-1 was produced by cotransfection with a plasmid encoding VSV-G (pHIT/G) and the pNL-Luc-E$^-$R$^+$ or pNL-Luc-E$^-$R$^-$ proviral clone (10). (10). The preparation and titration of viruses are described elsewhere (11). Briefly, the concentration of p24 antigen in the culture supernatant was measured using a p24 Gag antigen capture ELISA kit (ZeptoMetrix, Buffalo, NY). The infectivity of the prepared viral stock was examined using MAGIC5 cells. HT1080 cells were infected for 48 hours with viruses that had 200 ng/mL of p24 Gag antigen, giving a multiplicity of infection (MOI) of 0.7.

Immunostaining. Immunostaining was carried out as described (9). A rabbit polyclonal Rad51 antibody raised against the bacterially expressed protein and a mouse monoclonal antibody raised against synthesized peptides of full-length of Vpr (mAb8D1) were used as the primary antibody. Goat anti-rabbit IgG conjugated with Alexa Fluor 488 (Molecular Probes, Inc., Eugene, OR) and goat anti-mouse IgG conjugated with Cy3 (Zymed Laboratories, Inc., San Francisco, CA) were used as the secondary antibodies. Images were captured on a phase contrast microscope, BX50 (Olympus Corp., Tokyo Japan), or a Radiance 2100 laser scanning confocal microscope (Carl Zeiss, Oberkochen, Germany).

Overexpression and purification of Vpr and its mutant. The HIV-1 *vpr* gene was ligated into the *Nde*I and *Bam*HI sites of the pET15b vector (Novagen, Madison, WI). The Vpr protein and VprΔC12 mutant were produced in the *Escherichia coli* BL21 (DE3) Codon(+)RIL strain (Novagen) by induction with isopropyl-β-D-thiogalactopyranoside (IPTG; Nacalai Tesque, Inc., Kyoto, Japan) and were purified as described in Supplementary Method. The concentration of the purified Vpr protein was determined with a Bio-Rad protein assay kit (Bio-Rad Laboratories, Hercules, CA) using bovine serum albumin (BSA) as the standard.

Isolation of nuclei. Cells scraped from culture dishes were washed once with ice-cold PBS and resuspended in 3 mL of ice-cold 20 mmol/L Tris-HCl buffer (pH 7.6) containing 60 mmol/L KCl, 15 mmol/L NaCl, 5 mmol/L $MgCl_2$, 1 mmol/L DTT, 250 mmol/L sucrose, 0.6% NP40, and

Note: Supplementary data for this article are available at Cancer Research Online (http://cancerres.aacrjournals.org/).

Requests for reprints: Hitoshi Kurumizaka, Graduate School of Science and Engineering, Waseda University, 3-4-1 Okubo, Shinjuku-ku, 169-8555 Tokyo, Japan. Phone: 81-3-5286-8189; Fax: 81-3-5292-9211; E-mail: kurumizaka@waseda.jp and Yukihito Ishizaka, Department of Intractable Diseases, International Medical Center of Japan, 1-21-1 Toyama, Shinjuku-ku, 162-8655 Tokyo, Japan. Phone: 81-3-5272-7527; E-mail: zakay@ri.imcj.go.jp.

doi:10.1158/0008-5472.CAN-05-3144

protease inhibitor mixture (Sigma). The cell suspension was incubated for 10 minutes on ice and the sucrose concentration was adjusted to 1.6 mol/L. Then, the sample was loaded onto a sucrose cushion of 2.3 mol/L sucrose solution and centrifuged at 35,000 × *g* for 30 minutes. The isolated nuclei were obtained in the 2.3 mol/L sucrose fraction. For immunostaining, isolated nuclei were cytocentrifuged to the MAS-coated slide glass (Matsunami Glass IND., LTD., Tokyo, Japan) for 6 minutes at 800 rpm (Thermo Shandon, Chadwick Road, United Kingdom).

PFGE assay. Isolated nuclei were incubated with 10 μmol/L of purified Vpr or VprΔC12 for 15 hours at 30°C. The cells (isolated nuclei) were embedded in agarose plugs at a density of 3×10^5 cells/100 μL. The plugs were treated with proteinase K solution [0.5 mol/L EDTA (pH 8.0), 1% sarcosyl, and 0.5 mg/mL proteinase K] for 38 hours at 50°C. After PFGE was done in a CHEFF Mapper (Bio-Rad Laboratories), the gels were stained with Vistra Green (Amersham Bioscience, Piscataway, NJ).

The DNA-binding assay. The Vpr protein was incubated with ϕX174 single-stranded DNA (ssDNA; 20 μmol/L) or ϕX174 superhelical dsDNA (10 μmol/L) in 10 μL of 8 mmol/L Tris-HCl buffer (pH 8.5) containing 1 mmol/L DTT and 100 μg/mL BSA. The reaction mixtures were incubated for 1 hour at 37°C and were analyzed by electrophoresis on a 0.8% agarose gel in 1× TAE buffer (40 mmol/L Tris acetate and 1 mmol/L EDTA) at 3.3 V/cm for 2 hours. The bands were visualized using ethidium bromide staining.

Nuclease activity. The Vpr protein (18.8 μmol/L) or DNaseI (Invitrogen Corporation, Carlsbad, CA; 0.02 unit/μL) were incubated with ϕX174 superhelical double-stranded DNA (dsDNA; 2.5 μmol/L) in 40 μL of 15 mmol/L Tris-HCl buffer (pH 8.5) containing 1 mmol/L DTT and 100 μg/mL BSA, in the presence of 5 mmol/L $MgCl_2$, $MnCl_2$, $ZnSO_4$, or $CaCl_2$. The reaction mixtures were incubated at 37°C for 30 minutes. After incubation, the samples were treated with proteinase K (0.3 mg/mL) in the presence of 0.1% SDS and the DNA was extracted using phenol-chloroform. The DNA was precipitated by ethanol and was analyzed by electrophoresis on a 0.8% agarose gel in 1 × TAE buffer at 6.6 V/cm for 30 minutes. The bands were visualized with ethidium bromide staining.

The Ni-NTA agarose pull-down assay. Isolated nuclei were disrupted in 20 mmol/L Tris-HCl buffer (pH 8.5) containing 200 mmol/L KCl, 2 mmol/L 2-mercaptoethanol, 0.25 mmol/L EDTA, and 10% glycerol. The extract was incubated with His_6-Vpr (53 μmol/L) for 15 hours at 30°C. After incubation, His_6-Vpr was precipitated with 4 μL of Ni-NTA agarose beads and the beads were washed thrice with 500 μL of 20 mmol/L Tris-HCl buffer (pH 7.6) containing 100 mmol/L NaCl, 5 mmol/L DTT, 10 mmol/L imidazole, 1 mmol/L EDTA, and 0.2% Tween 20. The proteins precipitated with the Ni-NTA beads were analyzed by 16% SDS-PAGE. The bands were visualized by silver staining.

Results

Vpr expression induces chromosomal double-strand breaks. To test whether HIV-1 infection causes double-strand breaks, we used PFGE, which was able to clearly detect the double-strand breaks induced by X-ray irradiation (Fig. 1*A*, *lane 2*; ref. 12). HT1080 cells were infected with HIV-1 that had 200 ng/mL of p24 Gag antigen, giving a MOI of 0.7, and the cellular DNA was fractionated using PFGE. Figure 1*A* (*lane 6*) shows that HIV-1 infection induced double-strand breaks. Interestingly, the amount of HIV-1-dependent double-strand breaks was reduced significantly (Fig. 1*A*, *lane 5*) when the *vpr* gene was deleted from the HIV-1 viral genome (HIV-1ΔVpr). To show that HIV-1-dependent double-strand breaks are attributable to Vpr expression, we examined double-strand break formation in Vpr stable transfectant, MIT-23 (9), in which Vpr expression is controlled by the rtet promoter by doxycycline, and, in ΔVpr, a mock transfectant. As shown in Fig. 1*B*, double-strand breaks were observed in the Vpr-expressing cells (*lane 5, arrow*) but not in the mock transfectants (*lane 4*). Furthermore, Rad51 foci, which are formed

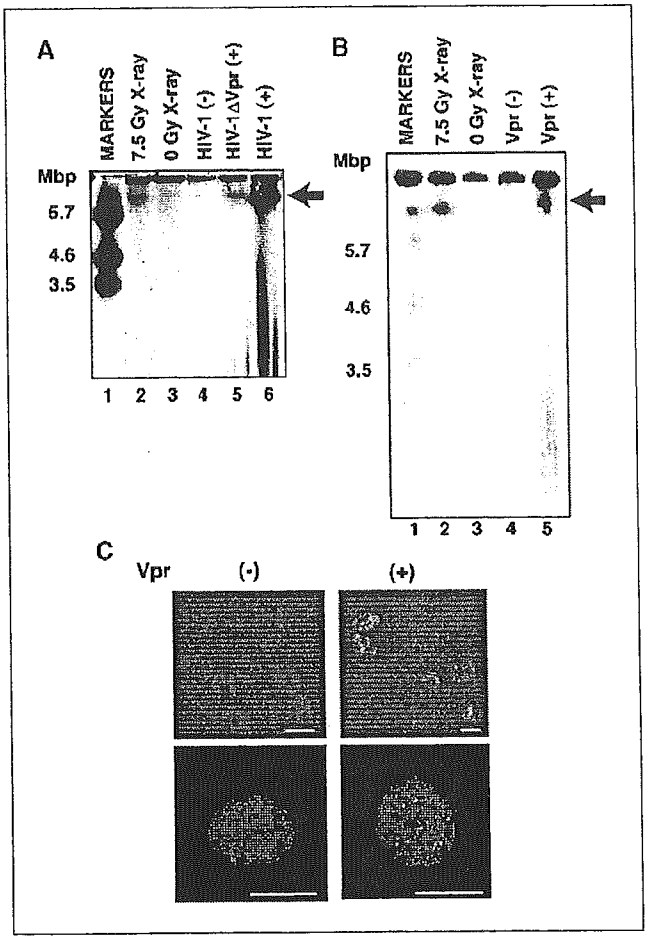

Figure 1. Vpr induces double-strand breaks *in vivo*. *A*, PFGE analysis of double-strand breaks after HIV-1 infection. HT1080 cells were infected with the same amount of HIV-1 or HIV-1ΔVpr (MOI = 0.7) and subjected to PFGE. As a positive control, uninfected cells were analyzed immediately after 7.5 Gy of X-ray irradiation. Molecular mass markers (*lane 1*), control cells (*lanes 3* and *4*), cells subjected to X-ray irradiation (*lane 2*), and cells infected with HIV-1ΔVpr (*lane 5*) or HIV-1 (*lane 6*) are shown. *Arrow*, position corresponding to the double-strand breaks. *B*, PFGE analysis in Vpr-expressing cells. Molecular mass markers (*lane 1*), cells irradiated with 7.5 Gy (*lane 2*), control cells (*lane 3*), mock transfectants (*lane 4*), and cells with Vpr expression (*lane 5*) are shown. *Arrow*, double-strand breaks. *C*, Rad51 focus formation with Vpr expression. An immunohistochemical analysis was used to detect Rad51 in cells with (*right*) or without (*left*) Vpr expression. Bar, 10 μm.

at double-strand break sites (13), were observed with Vpr expression (Fig. 1*C*). These results indicate that Vpr is responsible for double-strand break formation. The double-strand breaks shown in Fig. 1*B* were not the result of an apoptotic process as the DNA ladder typically observed in apoptotic cells (14) was not detected (data not shown).

Vpr has no endonuclease activity. Next, we studied whether Vpr directly induces double-strand breaks. The recombinant Vpr protein was purified to near homogeneity (Fig. 2*A*) and the DNA-binding activity of Vpr was examined. As shown in Fig. 2*B*, purified Vpr bound both ssDNA (*lanes 2-6*) and dsDNA (*lanes 8-12*) in an ATP- and Mg^{2+}-independent manner (15). Then, we examined whether Vpr has nuclease activity. Superhelical dsDNA containing small amounts of nicked circular dsDNA was incubated with Vpr in the presence of various divalent cations. After the incubation, the proteins were removed and the DNA was examined by

electrophoresis. If Vpr induces a double-strand break or nick, the superhelical dsDNA would give rise to linear or nicked circular forms, producing a different electrophoretic pattern. However, the DNA incubated with Vpr in the absence (*lane 2*) or presence of any divalent cation examined (*lanes 4, 6, 8,* and *10*) showed the same migration pattern with control (*lane 1*), indicating that Vpr does not cleave DNA (Fig. 2*C*). Positive control experiments showed that the DNA was digested by DNaseI with $MgCl_2$, $MnCl_2$, or $CaCl_2$ (*lanes 5, 7,* and *11*) but not with $ZnSO_4$ (*lane 9*; Fig. 2*C*). Therefore, these results indicate that Vpr lacks endonuclease or nicking activity.

Vpr induces double-strand breaks *in vitro*. In a second approach, we tested whether purified Vpr induces double-strand breaks in nuclei isolated from HT1080 cells (Fig. 3*A*). First, we confirmed by a laser confocal microscopy that Vpr localizes in nuclei after incubation *in vitro* (Fig. 3*B*). The nuclear DNA was then analyzed for double-strand breaks by using PFGE (Fig. 3*C*). Interestingly, purified Vpr induced double-strand breaks in the DNA of the isolated nuclei (Fig. 3*C*, *lane 5, arrow*). By contrast, few double-strand breaks were detected without Vpr (Fig. 3*C*, *lane 4*). Because Vpr alone did not show endonuclease activity (Fig. 2*C*), these results suggest that Vpr interacts with intrinsic nuclear protein(s), which required for double-strand break formation. To identify candidates for the Vpr-interacting nuclear proteins, we did the Ni-NTA pull-down assay. In this assay, recombinant His_6-tagged Vpr was incubated with the extract from isolated nuclei and Ni-NTA beads precipitated proteins bound to His_6-tagged Vpr (Fig. 3*D*). As shown in Fig. 3*D*, His_6-tagged Vpr associated with numerous proteins that were not detected in the control precipitates (*lane 2, asterisks*).

The DNA-binding activity of Vpr is correlated with double-strand break formation. The COOH-terminal region of Vpr is arginine rich and is thought to be an important site for DNA binding to Vpr (15). Nuclear magnetic resonance analysis shows that Vpr has three α-helixes (amino acids 17-33, 38-50, and 56-77) in solution, whereas the COOH-terminal region from amino acid residues 84 to 96 is disordered (16). This suggests that the deletion of the COOH-terminal 12 amino acid residues does not affect the tertiary structure of Vpr. We purified a Vpr mutant protein lacking the COOH-terminal 12-amino-acid residues (VprΔC12; Fig. 4*A*), and examined its DNA-binding activity. Purified VprΔC12 was significantly defective in both ssDNA- and dsDNA-binding activity compared with wild-type Vpr (Fig. 4*B*). Interestingly, VprΔC12 induced double-strand breaks in isolated nuclei but its efficiency was reduced significantly (Fig. 4*C*, *lane 6*). These results indicate that the DNA-binding ability of Vpr is important for the induction of double-strand breaks by Vpr.

Discussion

Here, we present evidence that HIV-1 Vpr induces double-strand breaks. Our data are consistent with previous observations in Vpr-expressing cells: the up-regulation of gene amplification events that are believed to be introduced by broken DNA strands (17) and the activation of activating Rad3-related/ataxia-telangiectasia mutated, followed by the phosphorylation of their downstream substrate, a histone H2A variant, H2AX, and γ-H2AX and BRCA1 focus formation (8). Biochemical analyses using purified Vpr indicated that Vpr alone has no endonuclease activity (Fig. 2*C*), suggesting that a cellular factor(s), possibly with endonuclease activity, is required for Vpr-dependent double-strand breaks. The factor(s) required for double-strand breaks must preexist in nuclei because double-strand breaks were observed upon incubating a mixture of isolated nuclei and purified Vpr *in vitro* (Fig. 3*C*). As one possible mechanism, Vpr may recruit a nuclease factor to chromosomal DNA, given that the Vpr-dependent double-strand breaks were correlated with the DNA-binding activity (Figs. 4*B* and *C*). Alternatively, Vpr itself may acquire endonuclease activity after modification in the nucleus. Further analyses are necessary to clarify this point.

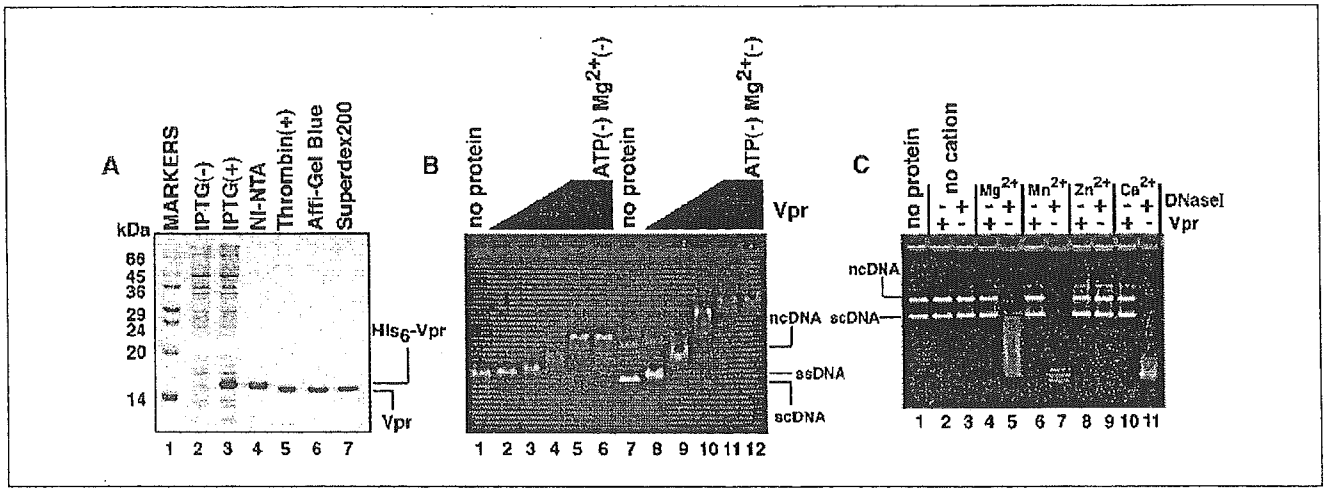

Figure 2. The Vpr-DNA interaction *in vitro*. *A*, purification of recombinant Vpr. Proteins from each purification step were analyzed using 16% SDS-PAGE with Coomassie brilliant blue staining. Molecular mass markers (*lane 1*), whole-cell lysates before (*lane 2*) and after (*lane 3*) induction with IPTG, samples from the Ni-NTA fraction (*lane 4*), the fraction after removing the hexahistidine tag (*lane 5*), the Affi-Gel Blue fraction (*lane 6*), and the Superdex 200 fraction (*lane 7*) are shown. *B*, the DNA-binding activity of Vpr. ϕX174 circular ssDNA (20 μmol/L; *lanes 2-6*) and ϕX174 superhelical dsDNA (*scDNA*; 10 μmol/L; *lanes 8-12*) containing a small amount of nicked circular DNA (*ncDNA*) were incubated with Vpr in the presence of 1 mmol/L ATP and 1 mmol/L $MgCl_2$. Control experiments without ATP and $MgCl_2$ (*lanes 6* and *12*) are included. The Vpr concentrations were 1.25 μmol/L (*lanes 2* and *8*), 2.5 μmol/L (*lanes 3* and *9*), 5 μmol/L (*lanes 4* and *10*), and 10 μmol/L (*lanes 5, 6, 11,* and *12*). *Lanes 1* and *7*, negative controls without protein. *C*, nuclease activity. ϕX174 scDNA (2.5 μmol/L) was incubated with Vpr (18.8 μmol/L; *lanes 2, 4, 6, 8,* and *10*) or DNaseI (*lanes 3, 5, 7, 9,* and *11*) in the absence of divalent cation (*lanes 2* and *3*) or in the presence of 5 mmol/L $MgCl_2$ (*lanes 4* and *5*), 5 mmol/L $MnCl_2$ (*lanes 6* and *7*), 5 mmol/L $ZnSO_4$ (*lanes 8* and *9*), or 5 mmol/L $CaCl_2$ (*lanes 10* and *11*). *Lane 1*, negative control without protein.

In the HIV-1 life cycle, DNA breakage and repair are thought to be essential steps for integrating the double-stranded viral cDNA into the host genome. In this study, we found that Vpr is one molecule responsible for the double-strand breaks that occur upon HIV-1 infection. However, it is also noteworthy that some double-strand breaks were induced in the cells with HIV-1ΔVpr (Fig. 1*A*, *lane 5*), suggesting that other viral factors are also involved. It has been shown that integrase activates the ataxia-telangiectasia mutated–dependent pathway (7) and, thus, the double-strand breaks observed with HIV-1ΔVpr infection are probably owing to integrase. For viral integration to occur, the amount of double-strand breaks induced by HIV-1ΔVpr (Fig. 1*A*, *lane 5*) may be sufficient, because viral production in peripheral blood mononuclear cells was not alleviated by infection with

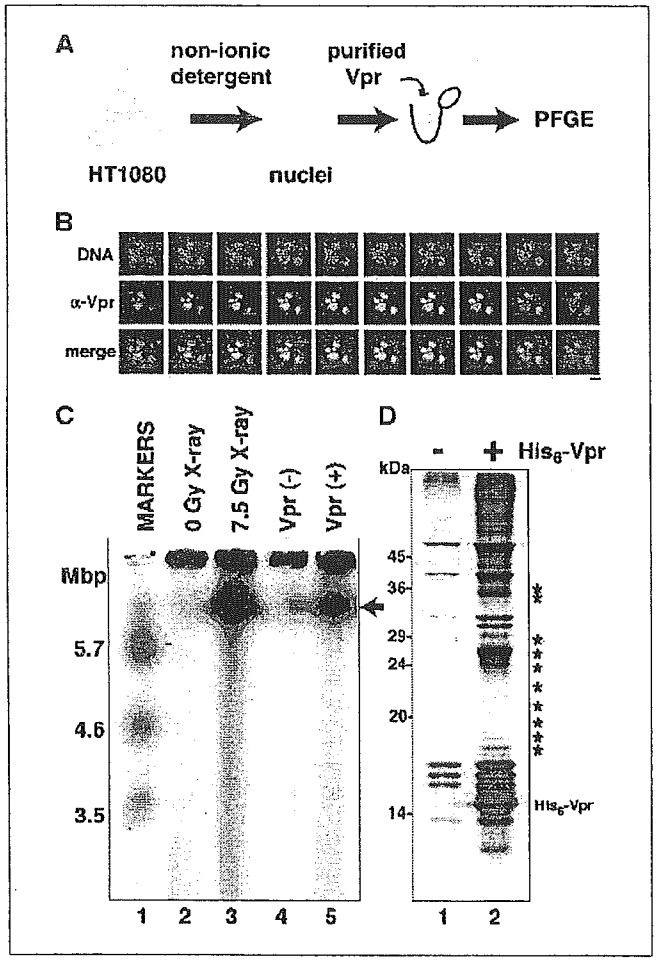

Figure 3. Purified Vpr induces double-strand breaks *in vitro*. *A*, a scheme of the protocol used to detect Vpr-induced double-strand breaks in isolated nuclei. *B*, Vpr localization in isolated nuclei. Isolated nuclei from HT1080 after incubation with Vpr were immunostained by α-Vpr (mAb8D1) and the images were captured by a laser confocal microscopy. The Z-series of optical sections collected at 1 μm steps of the cells were presented. Vpr (*red; middle*), DNA staining by Hoechst (*blue; top*) and their merged images (*bottom*) are shown. Without Vpr incubation, any signals by α-Vpr immunostaining were not detected in isolated nuclei (data not shown). Bar, 10 μm. *C*, PFGE analysis of double-strand breaks in isolated nuclei treated with Vpr. Molecular mass markers (*lane 1*), control cells (*lane 2*), cells subjected to X-ray irradiation (*lane 3*), and isolated nuclei without (*lane 4*) or with 10 μmol/L Vpr (*lane 5*). *Arrow*, double-strand breaks. *D*, Ni-NTA pull-down assay with His_6-tagged Vpr on isolated nuclei. Precipitated proteins bound to His_6-tagged Vpr (*lane 2*) and the control precipitates (*lane 1*) are indicated. *, His_6-Vpr–specific bands.

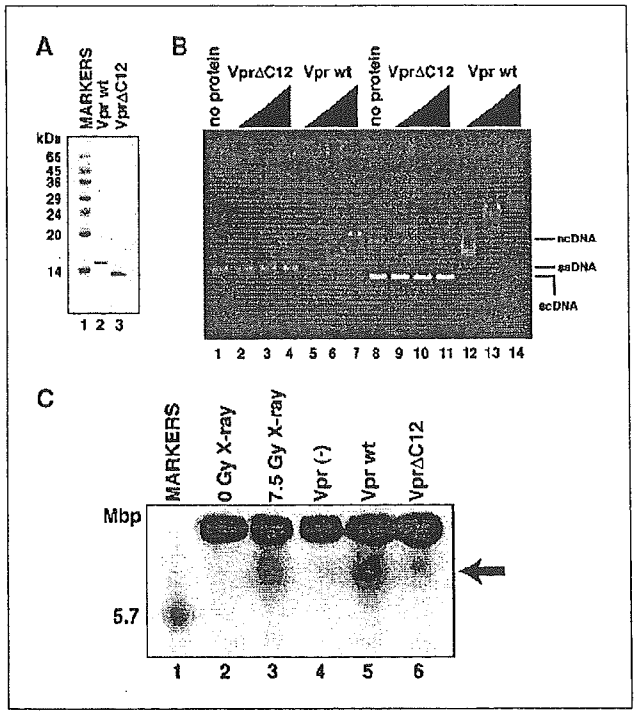

Figure 4. DNA-binding and double-strand break formation by Vpr. *A*, purification of VprΔC12. Purified VprΔC12 was analyzed using 16% SDS-PAGE with Coomassie brilliant blue staining. *Lane 1*, molecular mass markers. *Lanes 2* and *3*, purified wild-type Vpr and VprΔC12 protein, respectively. *B*, the DNA-binding activity of VprΔC12. The DNA-binding experiments were done using the protocol used to obtain Fig. 2*B*. The concentrations of VprΔC12 were 2.5 μmol/L (*lanes 2* and *9*), 5 μmol/L (*lanes 3* and *10*), and 10 μmol/L (*lanes 4* and *11*), and those of the wild-type Vpr were 2.5 μmol/L (*lanes 5* and *12*), 5 μmol/L (*lanes 6* and *13*), and 10 μmol/L (*lanes 7* and *14*). Negative controls without protein (*lanes 1* and *8*) are included. *C*, PFGE analysis of double-strand breaks in isolated nuclei treated with Vpr or VprΔC12. Molecular mass marker (*lane 1*), cells without (*lane 2*) or with (*lane 3*) 7.5 Gy of X-ray irradiation, control nuclei (*lane 4*), nuclei with Vpr (*lane 5*), and nuclei with VprΔC12 (*lane 6*). Vpr was used at 10 μmol/L. *Arrow*, double-strand breaks.

Vpr-deleted HIV-1 (18).[4] Vpr-induced double-strand breaks may be surplus to those required for viral integration (Fig. 1*A*, *lane 6*). The resultant DNA damage may reduce the integrity of the host genome.

Recently, DNA damage signaling was observed at an early stage of tumor development, suggesting that the DNA damage response is a mechanism to prevent the progression of pre-neoplasic lesions (5). If DNA repair is not accomplished correctly or is skipped because of unregulated checkpoint controls, the genomic structure would be altered severely (19). The progression of malignant tumors in AIDS-defining cancers is well documented in oncovirus infections (1, 2). If DNA damage increases the probability of neoplasia, Vpr-induced double-strand breaks with oncovirus infection may accelerate tumor progression during the clinical course of AIDS. In addition to AIDS-defining cancers, non-AIDS-defining cancers also occur at a higher incidence and the factor responsible for such oncogenesis is now a critical issue (3, 4). Vpr-induced DNA damage may result in

[4] M. Shimura, unpublished data.

these AIDS-related malignancies. It is essential to explore the molecular mechanism of Vpr-induced double-strand breaks to clarify their role in HIV-1 infection and their effect on the stability of the host cell genome.

Acknowledgments

Received 9/1/2005; revised 11/16/2005; accepted 11/22/2005.

Grant support: Grants-in-Aid for Scientific Research from the Ministry of Health, Labor, and Welfare of Japan; the Japanese Society for the Promotion of Science; the Ministry of Education, Sports, Culture, Science, and Technology of Japan; and a research grant from the Kato Memorial Trust for Nambyo Research and the Japan Health Sciences Foundation.

The costs of publication of this article were defrayed in part by the payment of page charges. This article must therefore be hereby marked *advertisement* in accordance with 18 U.S.C. Section 1734 solely to indicate this fact.

We thank Dr. Masashi Tatsumi (National Institute of Infectious Diseases, Tokyo, Japan) for providing us with MAGIC5 cells and Koji Nakatani for his technical assistance and heart-warming support.

References

1. Beral V, Peterman T, Berkelman R, Jaffe H. AIDS-associated non-Hodgkin lymphoma. Lancet 1991;337:805–9.
2. Bellan C, De Falco G, Lazzi S, Leoncini L. Pathologic aspects of AIDS malignancies. Oncogene 2003;22:6639–45.
3. Wistuba II, Behrens C, Gazdar AF. Pathogenesis of non-AIDS-defining cancers: a review. AIDS Patient Care STDS 1999;13:415–26.
4. Chiao EY, Krown SE. Update on non-acquired immunodeficiency syndrome-defining malignancies. Curr Opin Oncol 2003;15:389–97.
5. Bartkova J, Horejsi Z, Koed K, et al. DNA damage response as a candidate anti-cancer barrier in early human tumorigenesis. Nature 2005;434:864–70.
6. Gorgoulis VG, Vassiliou L-VF, Karakaidos P, et al. Activation of the DNA damage checkpoint and genomic instability in human precancerous lesions. Narture 2005;434:907–13.
7. Lau A, Swinbank KM, Ahmed PS, et al. Suppression of HIV-1 infection by a small molecule inhibitor of the ATM kinase. Nat Cell Biol 2005;7:493–500.
8. Zimmerman ES, Chen J, Andersen JL, et al. Human immunodeficiency virus type 1 Vpr-mediated G_2 arrest requires Rad17 and Hus1 and induces nuclear BRCA1 and γ-H2AX focus formation. Mol Cell Biol 2004;24:9286–94.
9. Shimura M, Tanaka Y, Nakamura S, et al. Micronuclei formation and aneuploidy induced by Vpr, an accessory gene of human immunodeficiency virus type 1. FASEB J 1999;13:621–37.
10. Adachi A, Gendelman HE, Koenig S, et al. Production of acquired immunodeficiency syndrome-associated retrovirus in human and nonhuman cells transfected with an infectious molecular clone. J Virol 1986;59:284–91.
11. Tokunaga K, Greenberg ML, Morse MA, Cumming RI, Lyerly HK, Cullen BR. Molecular basis for cell tropism of CXCR4-dependent human immunodeficiency virus type 1 isolates. J Virol 2001;75:6776–85.
12. Krüger I, Rothkamm K, Löbrich M. Enhanced fidelity for rejoining radiation-induced DNA double-strand breaks in the G_2 phase of Chinese hamster ovary cells. Nucleic Acids Res 2004;32:2677–84.
13. Haaf T, Golub EI, Reddy G, Radding CM, Ward DC. Nuclear foci of mammalian Rad51 recombination protein in somatic cells after DNA damage and its localization in synaptonemal complexes. Proc Natl Acad Sci U S A 1995;92:2298–302.
14. Maecker HT, Hedjbeli S, Alzona M, Le PT. Comparison of apoptosis signaling through T cell receptor, fas, and calcium ionophore. Exp Cell Res 1996;222:95–102.
15. Zhang S, Pointer D, Singer G, Feng Y, Park K, Zhao LJ. Direct binding to nucleic acids by Vpr of human immunodeficiency virus type 1. Gene 1998;212:157–66.
16. Morellet N, Bouaziz S, Petitjean P, Roques BP. NMR structure of the HIV-1 regulatory protein VPR. J Mol Biol 2003;327:215–27.
17. Shimura M, Onozuka Y, Yamaguchi T, Hatake K, Takaku F, Ishizaka Y. Micronuclei formation with chromosome breaks and gene amplification caused by Vpr, an accessory gene of human immunodeficiency virus. Cancer Res 1999;59:2259–64.
18. Kawano Y, Tanaka Y, Misawa N, et al. Mutational analysis of human immunodeficiency virus type 1 (HIV-1) accessory genes: requirement of a site in the nef gene for HIV-1 replication in activated $CD4^+$ T cells *in vitro* and *in vivo*. J Virol 1997;71:8456–66.
19. Furuta S, Jiang X, Gu B, Cheng E, Chen PL, Lee WH. Depletion of BRCA1 impairs differentiation but enhances proliferation of mammary epithelial cells. Proc Natl Acad Sci U S A 2005;102:9176–81.